CERN-EP-2023-180
24 August 2023

Search for jet quenching effects in high-multiplicity pp collisions at $\sqrt{s} = 13$ TeV via di-jet acoplanarity

ALICE Collaboration*

Abstract

The ALICE Collaboration reports a search for jet quenching effects in high-multiplicity (HM) proton–proton collisions at $\sqrt{s} = 13$ TeV, using the semi-inclusive azimuthal-difference distribution $\Delta\phi$ of charged-particle jets recoiling from a high transverse momentum (high- $p_{T,\text{trig}}$) trigger hadron. Jet quenching may broaden the $\Delta\phi$ distribution measured in HM events compared to that in minimum bias (MB) events. The measurement employs a $p_{T,\text{trig}}$ -differential observable for data-driven suppression of the contribution of multiple partonic interactions, which is the dominant background. While azimuthal broadening is indeed observed in HM compared to MB events, similar broadening for HM events is observed for simulations based on the PYTHIA 8 Monte Carlo generator, which does not incorporate jet quenching. We elucidate the origin of the broadening by comparing biases induced by HM selection in the data and simulations, and discuss its implications for the study of jet quenching in small collision systems.

arXiv:2309.03788v1 [hep-ex] 30 Aug 2023

1 Introduction

Strongly-interacting matter at extreme temperature and density forms quark–gluon plasma (QGP), a state in which the dominant degrees of freedom are sub-hadronic [1, 2]. The QGP filled the early universe, and it is generated today in the collision of heavy atomic nuclei at the Relativistic Heavy Ion Collider (RHIC) at Brookhaven National Laboratory and at the Large Hadron Collider (LHC) at CERN. Measurements at these facilities, and their comparison with theoretical calculations based on viscous relativistic hydrodynamics, show that the QGP exhibits complex collective behavior, flowing with very low specific shear viscosity [3].

A key question in the experimental study of the QGP is the limit of its formation in terms of the size of the colliding nuclei. To explore this question, measurements have been carried out for “small collision systems”, in which one of the projectiles is a proton or light nucleus and the other a heavy nucleus, additionally with selection of high event activity (EA) such as produced particle multiplicity or forward neutron production (see e.g. Ref. [4]). Final-state hadronic distributions in small systems exhibit experimental signatures which are associated with production of the QGP in heavy-ion collisions [5], including collective flow [6–9] and enhancement in the production of strange hadrons [10].

Jets are the hadronic remnants of hard (high momentum transfer Q^2) interactions of quarks and gluons from the hadronic projectiles. Measurements of jet production and jet structure in elementary collisions are well described by theoretical calculations based on perturbative QCD (pQCD) [11–13]. In heavy-ion collisions, jets interact with the QGP, resulting in modifications of jet production rates, structure, and angular distributions, which provide incisive probes of the QGP (“jet quenching”) [14, 15].

Jet quenching is a necessary consequence of QGP formation in small systems, though its effects are expected to be small [16–22]. A common signature of jet quenching is the suppression of inclusive hadron or jet yield measured in heavy-ion collisions compared to that expected by scaling the corresponding yield measured in minimum-bias (MB) pp collisions, using a Glauber modeling of the collision geometry [14, 15, 23]. Inclusive jet yield suppression has been reported using this approach in EA-selected d–Au collisions at RHIC (EA based on forward multiplicity) [24] and in p–Pb collisions at the LHC (EA based on forward transverse energy E_T) [25]. However, Glauber modeling using these EA metrics in small systems is subject to significant non-geometric bias [4, 22, 26–32]. An alternative choice for the EA metric, based on zero-degree neutron measurements (nZDC), is found to be less biased, though the scaling still has model-dependent assumptions and uncertainties [4]. Such biases and uncertainties limit the sensitivity of the measurement of jet quenching effects in small systems using Glauber-scaled inclusive yield observables. At present there is no significant evidence, beyond experimental uncertainties, of jet quenching in small systems using this approach [33–35].

The PHENIX Collaboration has recently searched for jet quenching in d–Au collisions at a center-of-mass energy per nucleon–nucleon collision $\sqrt{s_{NN}} = 200$ GeV by the measurement of both π^0 and direct photon (γ_{dir}) inclusive yields in collisions selected by EA [32]. Jet quenching is studied using the γ_{dir} inclusive yield to estimate empirically the rate of hard processes, which does not depend upon Glauber scaling. Strong suppression in the ratio of π^0 and γ_{dir} inclusive yields is observed for high-EA relative to MB collisions, though with absolute value that is consistent with unity within the normalization uncertainty.

An alternative approach has been proposed to search for medium-induced inclusive yield suppression in small systems utilizing MB collisions of light nuclei [19, 20], which likewise does not require Glauber modeling for the yield scaling. However, this approach cannot be applied to EA-selected event populations in small collision systems, where the strongest signals characteristic of collective flow have been observed [6–10].

The comprehensive search for jet quenching effects in small collision systems therefore also requires

approaches based on coincidence observables, which are self-normalized and likewise do not require a Glauber model calculation of nuclear geometry for an EA-selected population. The measurement of jets recoiling from a high- p_T hadron trigger in p–Pb collisions at $\sqrt{s_{NN}} = 5.02$ TeV has set a limit of 0.4 GeV/ c (90% confidence) for medium-induced energy transport to angles greater than 0.4 radians relative to the jet axis, for high-EA collisions selected with criteria based both on forward multiplicity and on nZDC [36]. Measurement of the distribution of hadrons recoiling from a high- p_T jet trigger in EA-selected (nZDC) p–Pb collisions at $\sqrt{s_{NN}} = 5.02$ TeV likewise finds no significant jet quenching signal within uncertainties [37]. The measurement of azimuthal anisotropy of high- p_T hadrons finds small but non-zero second Fourier coefficient v_2 for events selected by EA based on forward E_T [38], though such effects cannot be attributed solely to jet quenching.

It therefore remains an open question whether the collective effects observed in small systems are indeed due to QGP formation, or whether they arise from other phenomena [22, 39–41]. New searches for jet quenching effects in small systems are required to resolve this issue.

In this article we present a novel search for jet quenching effects in EA-selected high-multiplicity (HM) pp collisions at $\sqrt{s} = 13$ TeV. Since “collision geometry” is ill-defined for EA-selected pp collisions, inclusive observables are not appropriate for such a search. Rather, we utilize the semi-inclusive hadron+jet acoplanarity observable [36, 42, 43], i.e. the distribution of the azimuthal angle $\Delta\phi$ between a high- p_T hadron trigger and correlated recoil jets, comparing $\Delta\phi$ measurements in HM-selected and MB populations. Jets are reconstructed from charged particles using the anti- k_T algorithm [44] with resolution parameter $R = 0.4$. Jet quenching in the QGP is expected to broaden the $\Delta\phi$ distribution relative to that in vacuum, due to in-medium multiple scattering [45–50]. However, at present there is no theoretical guidance for the magnitude of the jet transport parameter \hat{q} [14] or alternative characterizations of jet quenching in EA-selected pp collisions, and this is therefore entirely an experiment-driven search.

The analysis is based on the Δ_{recoil} observable developed for semi-inclusive measurements in [42], which provides data-driven suppression of uncorrelated background yield through the difference of trigger hadron-normalised recoil jet distributions in two exclusive trigger p_T intervals (Sec. 5). Precise suppression of uncorrelated background yield is crucial in this analysis, since the yield of uncorrelated recoil jets generated by multiple partonic interactions (MPI) from independent high- Q^2 processes can mimic azimuthal broadening arising from jet quenching. For the HM population we utilize a large data sample recorded by ALICE with an online HM trigger during the 2016–2018 LHC pp runs at $\sqrt{s} = 13$ TeV. The $\Delta\phi$ distributions from the HM-selected and MB event populations are compared. The results are also compared to theoretical calculations.

The paper is organized as follows: Sec. 2 presents the data set and offline analysis; Sec. 3 presents characterization of event activity using forward multiplicity; Sec. 4 presents jet reconstruction; Sec. 5 presents the coincidence observable Δ_{recoil} ; Sec. 6 presents data corrections; Sec. 7 presents systematic uncertainties; and Sec. 8 presents the physics results and their interpretation.

2 Data set and offline analysis

The ALICE detector and its performance are described in Refs. [51, 52]. Data for this analysis were recorded during the 2016, 2017, and 2018 LHC runs with pp collisions at $\sqrt{s} = 13$ TeV. Events were selected online using signals in the V0 detectors [53], which are plastic scintillator arrays covering the pseudorapidity ranges $2.8 < \eta < 5.1$ (V0A) and $-3.7 < \eta < -1.7$ (V0C). The V0 signal is proportional to the total number of charged particles (multiplicity) in the detector acceptance. Two different V0 trigger configurations were employed, called minimum bias (labelled “MB”) and high multiplicity (“HM”). The MB trigger required the in-time coincidence of V0A and V0C signals, while the HM trigger required the sum of V0A and V0C signal amplitudes (denoted as V0M) to be at least five times larger than the mean signal amplitude in MB events (denoted as $\langle \text{V0M} \rangle$). The HM trigger selected 0.1% of MB events with

the largest value of V0M.

The EA is characterized offline by the scaled V0 signal, $V0M/\langle V0M \rangle = (V0A + V0C)/\langle V0A + V0C \rangle$, which is insensitive to changes in V0 gain in the different data-taking periods due to scintillator aging. It also provides ordering of events in terms of EA without the need for precise calculation of the absolute V0 signal in model calculations, for a well-defined comparison of such models with data. The value of $\langle V0M \rangle$ is calculated separately for each data-taking run lasting a few hours, as a function of the collision vertex position along the beam axis. The HM selection is further constrained in the offline analysis to the range $5 < V0M/\langle V0M \rangle < 9$. The lower bound of 5 is determined by the online HM trigger threshold, while the upper bound of 9 is determined by the range over which the $V0M/\langle V0M \rangle$ distributions for the three different measurement periods are consistent; higher values may be affected by residual, uncorrected pileup effects.

In the offline analysis, jets are measured at midrapidity using charged particles reconstructed with the ALICE central barrel detectors, covering the range $|\eta| < 0.9$. Track reconstruction is based on space points measured by the Inner Tracking System (ITS) and Time Projection Chamber (TPC) [52]. Primary event vertices are reconstructed offline based on global tracks, which are required to have space points in the Silicon Pixel Detector (SPD) forming the two innermost layers of the ITS. Accepted events are required to have the primary vertex within $|z_{\text{vtx}}| < 10$ cm, where z_{vtx} is the location of the vertex along the beam axis relative to the nominal center of the ALICE detector.

For MB-triggered events, the pileup rate due to multiple hadronic pp collisions in the same LHC bunch crossing is less than 3.5%. The pile-up contribution is suppressed offline by rejecting events with multiple reconstructed event vertices. As discussed in Sec. 5, the observable Δ_{recoil} used in the analysis provides data-driven suppression of uncorrelated background yield, which also includes residual pileup events that are not rejected by the multiple-vertex algorithm. After event selection, the data sets have an integrated luminosity of 32 nb^{-1} for the MB trigger and 10 pb^{-1} for the HM trigger.

During the data taking the ITS had non-uniform efficiency, and the analysis therefore utilizes hybrid tracks [13, 54] to achieve azimuthally uniform tracking response. Hybrid tracks consist of good quality global tracks with at least one hit in the SPD, and complementary tracks without SPD signals. To ensure good momentum resolution, the momentum of these complementary tracks is determined using the primary vertex as a constraint. Reconstructed tracks with $|\eta| < 0.9$ and $p_T > 0.15 \text{ GeV}/c$ are accepted for the analysis. Hybrid track reconstruction efficiency is 0.85 at $p_T = 1 \text{ GeV}/c$, 0.82 at $p_T = 10 \text{ GeV}/c$, and 0.74 at $p_T = 50 \text{ GeV}/c$. Tracking efficiencies for MB and HM events are similar. Primary-track momentum resolution is 0.7% at $p_T = 1 \text{ GeV}/c$, 1.3% at $p_T = 10 \text{ GeV}/c$, and 3.7% at $p_T = 50 \text{ GeV}/c$.

Simulations are utilized for data corrections and for comparison to theoretical calculations. The simulations are based on the PYTHIA 8 event generator [55] with Monash tune [56], and a detailed GEANT3 model [57] of the ALICE detector response, which includes production of secondary particles and realistic hit digitization. Events generated by PYTHIA 8 without detector effects are denoted ‘‘particle-level,’’ and such events passed through GEANT3 are denoted ‘‘detector-level.’’

For particle-level events, the V0A and V0C responses are determined by counting the number of charged particles in their acceptance. The coincidence requirement of the online trigger is modeled by requiring particle-level events to have particles in both V0A and V0C, while detector-level events are required to have GEANT-generated hits in both V0A and V0C. The MB events are used to calculate the V0M distributions at both detector and particle level.

3 V0M/ $\langle V0M \rangle$ distributions

Figure 1 shows the $V0M/\langle V0M \rangle$ probability distribution for MB pp collisions at $\sqrt{s} = 13$ TeV. The lower limit for HM event selection, $V0M/\langle V0M \rangle = 5$, is indicated by the red dashed-dotted line. The figure

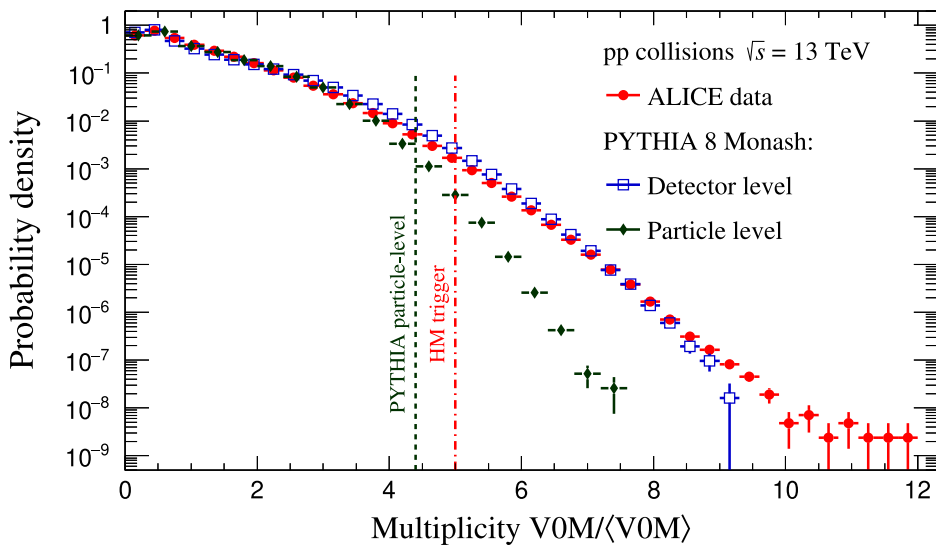


Figure 1: Probability distribution of $V0M/\langle V0M \rangle$ in MB pp collisions measured at $\sqrt{s} = 13$ TeV, and in simulated MB pp events generated by PYTHIA 8 at the particle and detector level. The vertical dashed lines indicate the lower bound for HM selection for data and particle-level simulations.

also shows the $V0M/\langle V0M \rangle$ probability distribution at the particle and detector level for PYTHIA 8-generated events for MB pp collisions at $\sqrt{s} = 13$ TeV. These distributions differ because of a large contribution at forward angles of secondary particles generated in detector material [58]. The particle-level distribution falls more rapidly than that observed in data in the range $V0M/\langle V0M \rangle > 4$. However, the detector-level distribution qualitatively reproduces that observed in data, with probability densities which lie within a factor ~ 2 of each other over a range of nine orders of magnitude in $V0M/\langle V0M \rangle$.

In order to compare PYTHIA 8 particle-level HM-selected distributions to data, we assume that the secondary particle yield due to interactions in detector material is on average proportional to the primary multiplicity in the V0 acceptance. The HM selection for the particle-level distribution is therefore chosen to select the same fraction of the MB cross section (0.1%) as the HM selection $V0M/\langle V0M \rangle > 5.0$ used for data. This selection corresponds to particle-level $V0M/\langle V0M \rangle > 4.4$, as indicated by the dark dashed line in Fig. 1.

4 Jet reconstruction

Several types of reconstructed jets are used in the analysis, which are distinguished using the notation defined in Refs. [36, 42]. For data, $p_{T,jet}^{raw,ch}$ refers to the raw output of the jet reconstruction algorithm; $p_{T,jet}^{reco,ch}$ refers to $p_{T,jet}^{raw,ch}$ after subtraction of the background contribution estimated as $\rho \times A_{jet}$, the product of median jet p_T density in the event and the jet area (Eq. 1); and $p_{T,jet}^{ch}$ refers to the fully corrected jet transverse momentum. For simulations, $p_{T,jet}^{part}$ refers to charged-particle jets at the particle level, and $p_{T,jet}^{det}$ charged-particle jets at the detector level; both quantities are corrected by $\rho \times A_{jet}$ using the following procedure.

Jets are reconstructed from accepted charged-particle tracks. Particles are assumed to be massless and their four-momenta are combined with the boost-invariant p_T recombination scheme [59]. Jet reconstruction is carried out twice for each event. The first reconstruction pass uses the k_T algorithm [59] with $R = 0.4$ and accepts jets with $|\eta_{jet}| < 0.9 - R$. The first-pass jet population is used to determine ρ , the event-wise estimate of the background energy density [60],

$$\rho = \text{median} \left\{ \frac{p_{T,\text{jet}}^{\text{raw},i}}{A_{\text{jet}}^i} \right\}, \quad (1)$$

where $p_{T,\text{jet}}^{\text{raw},i}$ and A_{jet}^i are the raw jet p_T and the area [61] of the i^{th} jet in the event. Jet area is calculated using the ghost area method of FastJet, with a ghost area of 0.005 [61]. The two hardest jets in the event are excluded from the median calculation. The most probable value of ρ is zero in both the MB and HM populations, while the mean value of ρ is 0.09 GeV/ c for MB and 1.24 GeV/ c for HM-selected events. For events containing a charged track in $|\eta| < 0.9$ with $20 < p_T < 30$ GeV/ c , the mean value of ρ is 0.39 GeV/ c for MB and 1.62 GeV/ c for HM events.

The second reconstruction pass uses the anti- k_T algorithm [59] with $R = 0.4$. The acceptance for the second pass is likewise $|\eta_{\text{jet}}| < 0.9 - R$ over the full azimuth.

The jet p_T obtained from the second pass is then adjusted for the median background p_T density ρ according to [60]

$$p_{T,\text{jet}}^{\text{reco,ch}} = p_{T,\text{jet}}^{\text{raw,ch}} - \rho \times A_{\text{jet}}. \quad (2)$$

The jet p_T scale and jet p_T resolution are the same as in Ref. [62].

5 Observables and raw data

The analysis utilizes a differential observable based on the semi-inclusive distribution of charged-particle jets recoiling from a high- p_T trigger (“h+jet”) [42] (see also [36, 43]). The key components of this approach are summarized in this section.

The goal of the analysis is the search for broadening of the $\Delta\phi$ distribution in HM-selected events due to medium-induced jet scattering, by comparison to the MB population. A significant source of background yield to this process arises from MPIs, in which multiple uncorrelated high- Q^2 partonic interactions occur in the same pp collision, with one such interaction generating a trigger hadron and another generating a recoil jet in the acceptance. The $\Delta\phi$ distribution of such MPI pairs is by definition uniform on average, thereby limiting the measurement sensitivity to broadening of the $\Delta\phi$ distribution from medium-induced scattering of correlated recoil jets.

Precise background yield correction must be carried out in a fully data-driven way, without model dependence. We therefore employ the Δ_{recoil} observable [42], which is the difference between semi-inclusive recoil jet distributions for two ranges of $p_{T,\text{trig}}$, both normalized to the number of trigger hadrons,

$$\Delta_{\text{recoil}}(p_T, \Delta\phi) = \frac{1}{N_{\text{trig}}} \frac{d^2 N_{\text{jet}}}{dp_{T,\text{jet}}^{\text{ch}} d\Delta\phi} \Bigg|_{p_{T,\text{trig}} \in \text{TT}_{\text{Sig}}} - c_{\text{Ref}} \times \frac{1}{N_{\text{trig}}} \frac{d^2 N_{\text{jet}}}{dp_{T,\text{jet}}^{\text{ch}} d\Delta\phi} \Bigg|_{p_{T,\text{trig}} \in \text{TT}_{\text{Ref}}}, \quad (3)$$

where TT denotes “trigger track.” In this analysis, $\text{TT}_{\text{Sig}} = \text{TT}\{20, 30\}$ specifies the range $20 < p_{T,\text{trig}} < 30$ GeV/ c for the Signal trigger distribution, and $\text{TT}_{\text{Ref}} = \text{TT}\{6, 7\}$ specifies the range $6 < p_{T,\text{trig}} < 7$ GeV/ c for the Reference trigger distribution. These intervals were chosen to optimize the opposing requirements of obtaining high statistical precision and limiting the kinematic range for more precise comparison of the same observables with different EA selections. The number of trigger hadrons measured in each TT class is denoted N_{trig} . The azimuthal difference $\Delta\phi$ between TT and recoil jet is defined to have the range $[0, \pi]$ radians.

The Δ_{recoil} distribution is a two-dimensional function of $p_{T,\text{jet}}$ and $\Delta\phi$ [36, 42]. We define its one-

dimensional projections, $\Delta_{\text{recoil}}(p_{T,\text{jet}})$ and $\Delta_{\text{recoil}}(\Delta\phi)$, onto the $p_{T,\text{jet}}^{\text{reco, ch}}$ and $\Delta\phi$ axes respectively, for restricted ranges in the other kinematic variable. These projections are shown in Figs. 2 and 3 both prior to and after corrections, as indicated by the functional argument (e.g. $\Delta_{\text{recoil}}(p_{T,\text{jet}}^{\text{reco, ch}})$ or $\Delta_{\text{recoil}}(p_{T,\text{jet}}^{\text{ch}})$).

The scaling factor c_{Ref} , which is applied to the Reference distribution (second term in Eq. 3), accounts for the different phase space available to observe uncorrelated yield in the Signal and Reference distributions [42, 43]. In this analysis, the value of c_{Ref} is determined from the ratio of trigger-normalized Signal and Reference recoil jet yields in the bin $0 < p_{T,\text{jet}}^{\text{reco, ch}} < 1$ GeV/c, which is expected to be dominated by background. This gives values $c_{\text{Ref}} = 0.95 \pm 0.03$ (syst.) in MB events and $c_{\text{Ref}} = 0.94 \pm 0.03$ (syst.) in HM events.

Since the uncorrelated yield is by definition independent of TT, it therefore contributes with equal magnitude to the two terms in Eq. 3 and is therefore removed by the subtraction. While Δ_{recoil} is a differential observable and not an absolutely normalized yield, its two terms are nevertheless calculable perturbatively [63]. Measurements of Δ_{recoil} in minimum-bias pp collisions are well described by PYTHIA 8 [36, 42].

In the analysis of both MB and HM-selected events, the dataset is divided into two statistically independent subsets, with the Signal distribution determined using 95% of all events, and the Reference distribution determined using the remaining 5%. These fractions were chosen to provide an equal number of trigger hadrons in the two TT classes, in order to optimize the statistical precision of Δ_{recoil} . The statistical error due to the N_{trig} normalization is negligible.

If two hadrons in an event satisfy the TT condition, one is chosen at random. This selection ensures that the p_T -differential TT distribution has the same shape as the inclusive charged-hadron yield, which is an essential requirement for a semi-inclusive measurement [42].

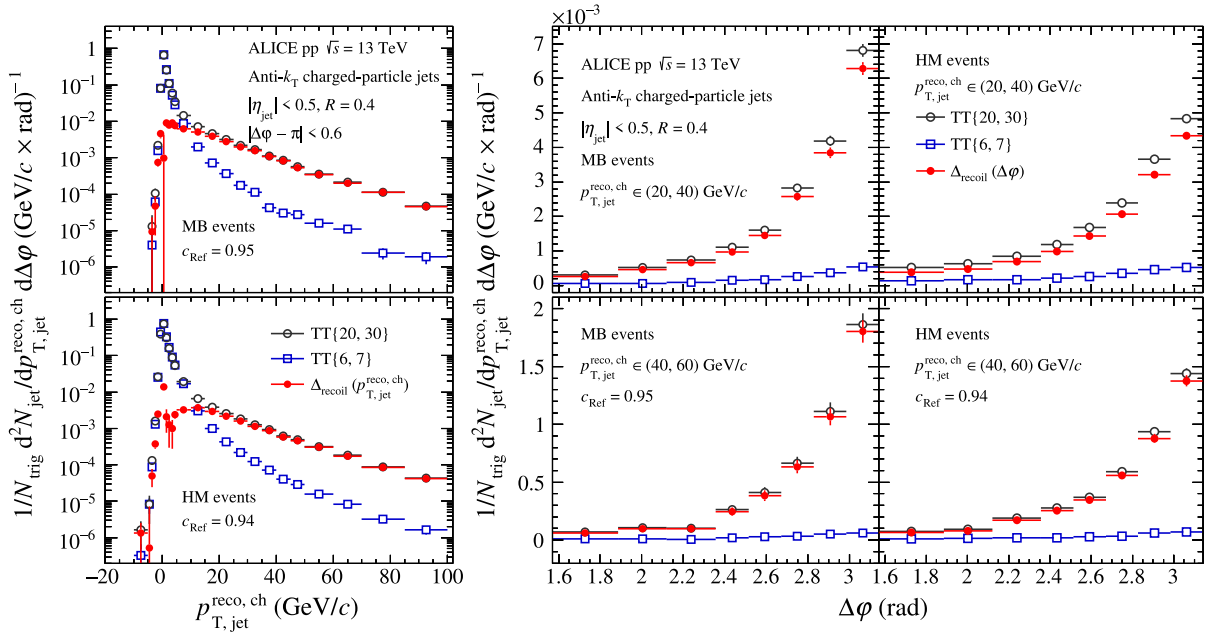


Figure 2: The Signal (TT{20,30}) and Reference (TT{6,7}) trigger-normalized recoil jet distributions and the corresponding Δ_{recoil} distribution for MB and HM pp collisions at $\sqrt{s} = 13$ TeV. Left panels: projection onto $p_{T,\text{jet}}^{\text{reco, ch}}$ for $|\Delta\phi - \pi| < 0.6$. Middle and right panels: projection onto $\Delta\phi$ in two $p_{T,\text{jet}}^{\text{reco, ch}}$ intervals.

Figure 2 shows selected $\Delta_{\text{recoil}}(p_{T,\text{jet}}^{\text{reco, ch}})$ and $\Delta_{\text{recoil}}(\Delta\phi)$ distributions, together with their corresponding Signal and Reference distributions. The Signal and Reference distributions have similar magnitude only in the region $p_{T,\text{jet}}^{\text{reco, ch}} < 20$ GeV/c, while at larger values of $p_{T,\text{jet}}^{\text{reco, ch}}$ the Reference distribution falls below the Signal distribution and Δ_{recoil} is similar in magnitude to the Signal distribution.

6 Corrections

Subtraction of the scaled Reference distribution in Eq. 3 accurately removes the uncorrelated jet yield [42]. However, the resulting Δ_{recoil} distribution is still subject to instrumental effects which smear $p_{\text{T,jet}}$ and $\Delta\phi$, whose correction is discussed in this section. These smearing effects are encoded in the four-dimensional response matrix R_{instr} , which maps the true (particle-level) distribution of Δ_{recoil} onto the measured distribution,

$$\Delta_{\text{recoil}}^{\text{Meas}}(\Delta\phi^{\text{det}}, p_{\text{T,jet}}^{\text{det}}) = R_{\text{instr}}(\Delta\phi^{\text{det}}, p_{\text{T,jet}}^{\text{det}}; \Delta\phi^{\text{part}}, p_{\text{T,jet}}^{\text{part}}) \otimes \Delta_{\text{recoil}}^{\text{True}}(\Delta\phi^{\text{part}}, p_{\text{T,jet}}^{\text{part}}). \quad (4)$$

Particle-level jets are clustered from all final-state charged particles generated with PYTHIA 8 as described in Sec. 2, except for weak decay daughters [64, 65], while detector-level jets are reconstructed from charged-particle tracks in the corresponding detector-level simulated events.

The $p_{\text{T,jet}}$ and angular smearing due to instrumental effects is very similar in the inclusive and recoil jet populations in these simulations. In addition, the inclusive population has a substantially larger sample in the simulated dataset. The matrix R_{instr} is therefore constructed using the inclusive jet population, by matching particle-level and detector-level jets in phase space within $\Delta R = \sqrt{(\Delta\eta)^2 + (\Delta\phi)^2} < 0.3$. The response matrix has p_{T} bins of width 1 GeV/ c , so that the difference in the spectrum shape of the inclusive and recoil jet populations has negligible effect on this procedure.

Track reconstruction efficiency, which is the dominant instrumental effect, is found to be the same for MB and HM events. The MB and HM analyses therefore use the same response matrix, obtained using MB events. Unmatched particle-level jets are tabulated and their rate is applied as an efficiency correction, following the unfolding correction discussed below. Jet matching efficiency for both MB and HM events is 0.98 at $p_{\text{T,jet}}^{\text{ch}} = 10$ GeV/ c and consistent with unity at higher $p_{\text{T,jet}}^{\text{ch}}$.

The corrected Δ_{recoil} distribution is calculated by regularized inversion of Eq. 4, using two-dimensional iterative Bayesian unfolding [66] implemented in the RooUnfold package [67]. The input distribution $\Delta_{\text{recoil}}^{\text{Meas}}$ is specified in the range $10 < p_{\text{T,jet}}^{\text{det}} < 100$ GeV/ c and $\pi/2 < \Delta\phi^{\text{det}} < \pi$ rad. The prior distribution for initiating the unfolding is the Δ_{recoil} particle-level spectrum calculated using PYTHIA 8 simulations. For unfolding the MB dataset, the prior is calculated using MB PYTHIA 8 events, whereas for unfolding the HM dataset the detector-level HM selection is applied to the simulated data, as shown in Fig. 1.

Regularization is optimized by requiring that the unfolded distributions from successive iterations exhibit a mean change of less than 2%, averaged over all p_{T} bins. The optimum number of iterations using this criterion is found to be 5, for both the MB and HM analyses.

While correction of the Δ_{recoil} distribution for instrumental effects is carried out by regularized unfolding using the full instrumental response matrix R_{instr} , insight into the unfolding procedure can also be gained by numerical characterization of the main smearing effects. Since the goal of this analysis is the search for broadening of the acoplanarity distribution in HM events, we focus here on azimuthal angular smearing, which is calculated event-by-event by the difference between particle-level and detector-level quantities. The observable $\Delta\phi$ is the azimuthal angular difference between the trigger track momentum vector and recoil jet centroid, both of which are smeared by instrumental effects. The angular smearing is found to have the same magnitude in MB and HM events. Azimuthal smearing of tracks contributing to TT{20,30} has RMS $\approx 2 \times 10^{-3}$ rad, while azimuthal smearing of the jet axis has RMS $\approx 26 \times 10^{-3}$ rad for $10 < p_{\text{T,jet}}^{\text{ch}} < 15$ GeV/ c and 11×10^{-3} rad for $60 < p_{\text{T,jet}}^{\text{ch}} < 80$ GeV/ c . The corresponding distributions of $\Delta\phi$ have RMS of 34×10^{-3} rad for $10 < p_{\text{T,jet}}^{\text{ch}} < 15$ GeV/ c and 13×10^{-3} rad for $60 < p_{\text{T,jet}}^{\text{ch}} < 80$ GeV/ c .

Subtraction of the reference distribution in the Δ_{recoil} observable corrects the uncorrelated background

yield. However, the resulting two-dimensional distribution as a function of $p_{T,\text{jet}}^{\text{ch}}$ and $\Delta\phi$ is still smeared by residual fluctuations of the uncorrelated background component. Correction for such fluctuations requires model assumptions (see e.g. Refs. [35,62]) and is therefore not included in the unfolding; rather, its magnitude is assessed for two common model choices and the variation in unfolded distributions is included in the systematic uncertainty, as discussed in Sec. 7.4.

The unfolding procedure is validated by a closure test in which the input is PYTHIA 8 detector-level events, the full analysis chain including unfolding is carried out, and the output is compared to the particle-level PYTHIA 8 spectrum. Good agreement between both distributions is found within statistical uncertainties, thereby confirming the robustness of the applied corrections.

7 Systematic uncertainties

The main sources of systematic uncertainty in the measurement of Δ_{recoil} are related to track reconstruction efficiency; track p_T resolution; the unfolding procedure; the determination of the scaling factor c_{Ref} ; and residual background fluctuations. The systematic uncertainty due to each source is estimated by varying the appropriate parameters and rerunning the full analysis chain.

However, the finite statistical precision of the data imposes a limit on the precision with which the spectrum can be unfolded. This limit is taken into account in the determination of the systematic uncertainties by using the following procedure, which is described in detail in Ref. [36]. For each parameter variation the spectrum is unfolded 10 times, with the central values of the spectrum varied randomly and independently using a Poisson distribution corresponding to the statistical error of each data point [36]. The ratio of the unfolded spectrum from each iteration to that of the primary analysis is calculated, and at each point the median of this set of ratios is assigned as the systematic uncertainty from this source. Tables 1 and 2 show representative values of the systematic uncertainty in $\Delta_{\text{recoil}}(p_{T,\text{jet}}^{\text{ch}})$ and $\Delta_{\text{recoil}}(\Delta\phi)$ measurements for MB and HM-selected event populations, respectively.

Table 1: Main sources of systematic uncertainty and total uncertainty in $\Delta_{\text{recoil}}(p_{T,\text{jet}}^{\text{ch}})$ and $\Delta_{\text{recoil}}(\Delta\phi)$ in representative bins, for MB events.

Projection	Relative systematic uncertainty (%)					
	$\Delta_{\text{recoil}}(p_{T,\text{jet}}^{\text{ch}})$ $ \Delta\phi - \pi < 0.6$		$\Delta_{\text{recoil}}(\Delta\phi)$ $p_{T,\text{jet}}^{\text{ch}} \in (20, 40)$ GeV/c		$\Delta_{\text{recoil}}(\Delta\phi)$ $p_{T,\text{jet}}^{\text{ch}} \in (40, 60)$ GeV/c	
	10–20 GeV/c	60–80 GeV/c	$2\pi/3$	π	$2\pi/3$	π
Tracking efficiency	0.2	7.1	3.7	1.9	8.4	5.6
Track p_T resolution	0.3	0.3	0.2	0.2	~ 0	0.3
Unfolding procedure	0.6	0.7	3.9	0.3	3.4	0.9
c_{Ref} variation	(-1.7, 1.9)	(-0.2, 0.2)	(-0.6, 0.7)	(-0.4, 0.4)	(-0.5, 0.5)	(-0.1, 0.2)
Bkgd fluctuations	(-1.6, 0)	(-2.4, 0)	(-4.7, 0)	(-1.6, 0)	(-5.0, 0)	(-2.7, 0)
Total uncertainty	(-2.5, 2.0)	(-7.6, 7.2)	(-7.2, 5.4)	(-2.5, 2.0)	(-10.4, 9.0)	(-6.3, 5.7)

7.1 Tracking efficiency and track p_T resolution

The tracking efficiency uncertainty is 3% [54]. To assess the corresponding uncertainty in the Δ_{recoil} distribution, a variation of R_{instr} is constructed in which 3% of all tracks are randomly discarded. While it is in practice not possible to generate R_{instr} with 3% higher tracking efficiency, this uncertainty is expected to be symmetric. The resulting uncertainty ranges from $< 1\%$ at low $p_{T,\text{jet}}^{\text{ch}}$ to 7% at high $p_{T,\text{jet}}^{\text{ch}}$, with only minor dependence on EA.

To assess the systematic uncertainty due to track p_T resolution, two different instances of R_{instr} are generated, with p_T -resolution corresponding to that of either real data or detector-level MC data hybrid

Table 2: Same as Tab. 1, for HM-selected events.

Projection	Relative systematic uncertainty (%)					
	$\Delta_{\text{recoil}}(p_{\text{T,jet}}^{\text{ch}})$ $ \Delta\phi - \pi < 0.6$		$\Delta_{\text{recoil}}(\Delta\phi)$ $p_{\text{T,jet}}^{\text{ch}} \in (20, 40) \text{ GeV}/c$		$\Delta_{\text{recoil}}(\Delta\phi)$ $p_{\text{T,jet}}^{\text{ch}} \in (40, 60) \text{ GeV}/c$	
	10–20 GeV/ c	60–80 GeV/ c	$2\pi/3$	π	$2\pi/3$	π
Tracking efficiency	0.6	7.6	4.2	1.9	7.1	5.2
Track p_{T} resolution	0.3	0.1	0.4	0.2	0.1	0.3
Unfolding procedure	0.9	0.7	5.7	1.6	2.6	1.2
c_{Ref} variation	(−4.5, 3.2)	(−0.3, 0.2)	(−1.5, 1.1)	(−0.6, 0.5)	(−1.3, 0.9)	(−0.3, 0.2)
Bkgd fluctuations	(−1.5, 0)	(−3.0, 0)	(−7.4, 0)	(−2.1, 0)	(−4.5, 0)	(−3.2, 0)
Total uncertainty	(−4.6, 3.7)	(−8.2, 7.6)	(−10.3, 7.2)	(−3.3, 2.5)	(−8.9, 7.6)	(−6.3, 5.4)

tracks. This source makes negligible contribution to the total systematic uncertainty.

7.2 Unfolding

The unfolding procedure has several parameters whose values influence the corrected Δ_{recoil} distribution: number of iterations; choice of prior spectrum; and range and binning of the raw input distribution. Each source was varied independently:

- The regularization condition was varied by ± 1 iterations with respect to the optimized value of 5. The corresponding uncertainty is found to be small, since unfolding converges rapidly to a stable result.
- Variations in the prior spectrum were obtained using the particle-level Δ_{recoil} spectra generated by the POWHEG MC event generator [68, 69] matched to PYTHIA 8 for parton shower and hadronization, and with different choices of regularization and factorization scale.
- The $p_{\text{T,jet}}$ binning was varied by shifting the bin boundaries by 1–2 GeV/ c , and by changing the lower bound of the input spectrum from 10 GeV/ c to 6 GeV/ c . The binning in $\Delta\phi$ was not varied, since $\Delta\phi$ smearing effects are small.

The systematic uncertainty attributed to unfolding is the maximum deviation in the Δ_{recoil} spectrum from varying these parameters, relative to the Δ_{recoil} spectrum using the primary analysis parameters. For $\Delta_{\text{recoil}}(p_{\text{T,jet}}^{\text{ch}})$, the resulting relative systematic uncertainty is about 0.6% for MB and 0.9% for HM events, with a weak dependence on $p_{\text{T,jet}}^{\text{ch}}$. For $\Delta_{\text{recoil}}(\Delta\phi)$, the relative systematic uncertainty is smallest at $\Delta\phi = \pi$ and increases monotonically towards $\Delta\phi = \pi/2$, for both MB and HM events.

7.3 Scaling factor c_{Ref}

The value of the c_{Ref} scaling factor in Eq. 3 was varied in the range [0.9, 1]. This range brackets the c_{Ref} values obtained by changing the $p_{\text{T,jet}}^{\text{reco, ch}}$ bin in which it is evaluated from (0, 1) GeV/ c to (−1, 0) GeV/ c , and by its variation with $\Delta\phi$. Different choices of c_{Ref} modify the Δ_{recoil} spectrum relative to that of the primary analysis result, with uncertainty decreasing as a function of $p_{\text{T,jet}}^{\text{ch}}$. Representative values are provided in Tables 1 and 2.

7.4 Background fluctuations

As discussed in Sec. 6, no correction is applied directly for the effect of residual background fluctuations; rather, a model-dependent estimate of its magnitude contributes to the systematic uncertainty. For this

estimate, a response matrix which encodes the effect of residual background fluctuations, R_{bkgd} , is convoluted with the instrumental response matrix R_{instr} in Eq. 4. The matrix R_{bkgd} is determined for events selected with $\text{TT}\{20, 30\}$, using two methods:

- Calculate the sum of track p_{T} in a cone $R = 0.4$ placed randomly in the acceptance, excluding overlap with the leading and sub-leading jets, and the TT. This sum is corrected for the median background density,

$$\delta p_{\text{T}}^{\text{RC}} = \sum_{\text{tracks} \in \text{RC}} p_{\text{T, track}} - \rho \times \pi R^2, \quad (5)$$

where πR^2 is the cone area and ρ is defined in Eq. 1. The matrix R_{bkgd} is the distribution of $\delta p_{\text{T}}^{\text{RC}}$.

- Embed a high- p_{T} track perpendicular in azimuth to the TT and at the same value of η , with p_{T} distributed uniformly in the range 0–20 GeV/ c . Jet reconstruction is then carried out, the jet candidate containing the embedded track is identified, and the quantity $\delta p_{\text{T}}^{\text{ET}}$ is calculated as

$$\delta p_{\text{T}}^{\text{ET}} = p_{\text{T, jet}}^{\text{ch, emb}} - \rho \times A_{\text{jet}}^{\text{emb}} - p_{\text{T}}^{\text{emb}}, \quad (6)$$

where $p_{\text{T}}^{\text{emb}}$ is transverse momentum of the embedded track. The matrix R_{bkgd} is the distribution of $\delta p_{\text{T}}^{\text{ET}}$.

Unfolding is then carried out for both choices, and the assigned systematic uncertainty is the maximum difference of the two unfolded Δ_{recoil} distributions from that of the primary analysis.

7.5 Total systematic uncertainty

The total systematic uncertainty of the unfolded Δ_{recoil} distribution is the quadrature sum of the contribution from each source. The systematic uncertainties from all sources except unfolding are correlated between the HM and MB analyses. This correlation is accounted for in the systematic uncertainty of ratios of Δ_{recoil} distributions by estimating the systematic uncertainty directly from the spread of the ratios calculated for each variation of the analysis configuration.

8 Results

8.1 Fully corrected distributions

Figure 3 shows fully-corrected distributions of $\Delta_{\text{recoil}}(p_{\text{T, jet}}^{\text{ch}})$ and $\Delta_{\text{recoil}}(\Delta\phi)$ measured in MB and HM-selected pp collisions at $\sqrt{s} = 13$ TeV, together with calculations based on PYTHIA 8, Monash tune, and a pQCD calculation at LO with Sudakov broadening [49, 70, 71] (the latter only for $\Delta_{\text{recoil}}(\Delta\phi)$ in MB collisions). Since the pQCD calculation is LO, there are large uncertainties in its normalization; the $\Delta_{\text{recoil}}(\Delta\phi)$ distributions from the calculation are therefore scaled to the integrated yield of the data in the same $p_{\text{T, jet}}^{\text{ch}}$ bin in order to compare their shapes. Both PYTHIA 8 and the pQCD calculation ($\Delta_{\text{recoil}}(\Delta\phi)$ shape only) are consistent with the distributions measured in MB events, within experimental uncertainties.

Comparison of the MB and HM $\Delta_{\text{recoil}}(p_{\text{T, jet}}^{\text{ch}})$ distributions reveals a yield suppression in HM collisions that is largely independent of $p_{\text{T, jet}}$, though there is a hint of a harder recoil jet spectrum for HM events. The mean value of the yield ratio HM/MB in the left panel of Fig. 3 is 0.78. The $\Delta_{\text{recoil}}(\Delta\phi)$ distributions show that the jet-yield suppression in HM events occurs predominantly in the back-to-back configuration, with the yield ratio HM/MB in the bin $\Delta\phi \sim \pi$ measured to be 0.69 for $20 < p_{\text{T, jet}}^{\text{ch}} < 40$ GeV/ c (Fig. 3, middle panel) and 0.78 for $40 < p_{\text{T, jet}}^{\text{ch}} < 60$ GeV/ c (Fig. 3, left panel). The total yield is suppressed, while the azimuthal distribution is broadened; such broadening could arise from jet quenching, i.e. medium-induced jet scattering occurs preferentially in HM events. Notably, however, PYTHIA 8 particle-level

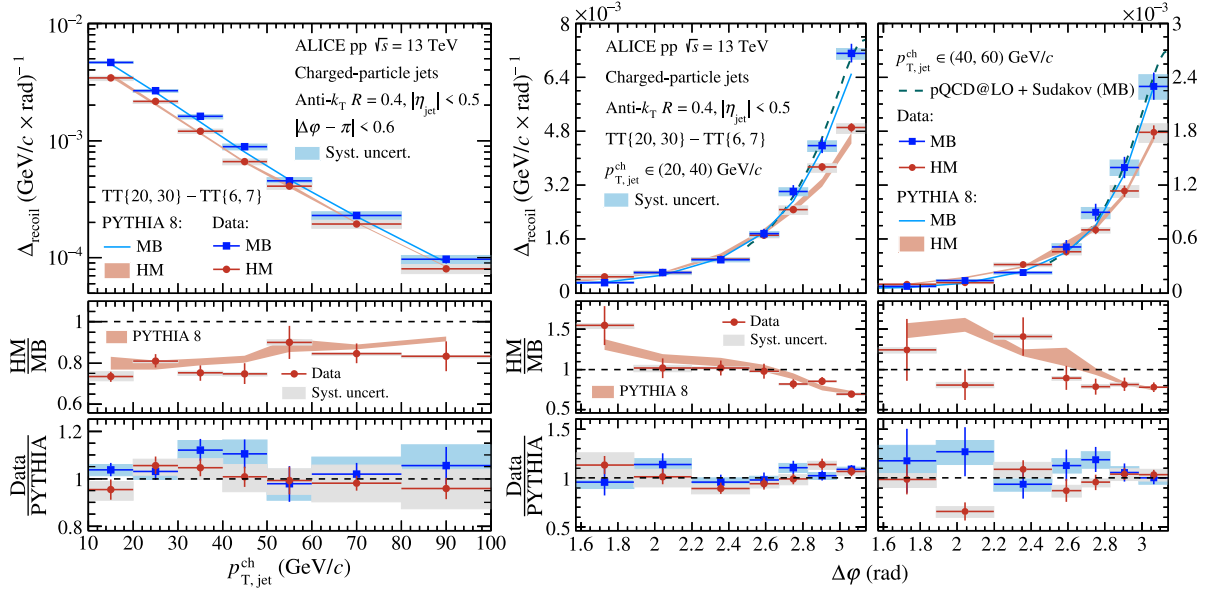


Figure 3: Fully-corrected Δ_{recoil} distributions measured in MB and HM-selected events in pp collisions at $\sqrt{s} = 13$ TeV. Left panel: $\Delta_{\text{recoil}}(p_{T,\text{jet}}^{\text{ch}})$ in $|\Delta\phi - \pi| < 0.6$; middle and right panels: $\Delta_{\text{recoil}}(\Delta\phi)$ for $20 < p_{T,\text{jet}}^{\text{ch}} < 40$ GeV/c and $40 < p_{T,\text{jet}}^{\text{ch}} < 60$ GeV/c. Also shown are particle-level simulated distributions calculated with PYTHIA 8 Monash tune, and a pQCD calculation at LO with Sudakov broadening [49, 70, 71] (MB $\Delta_{\text{recoil}}(\Delta\phi)$ only). The width of the PYTHIA 8 HM band represents the statistical uncertainty. Top row: Δ_{recoil} distributions; middle row: ratio of Δ_{recoil} distributions for HM/MB from data; bottom row: Data/PYTHIA 8 separately for MB and HM event selections.

distributions likewise exhibit jet yield suppression and azimuthal broadening for HM-selected events, accurately reproducing the measured distributions. Since PYTHIA 8 does not incorporate jet quenching, this disfavors jet quenching as the predominant effect generating the broadening seen in data.

8.2 Origin of HM induced TT-jet acoplanarity in PYTHIA 8

To clarify the origin of the broadening, a more detailed investigation is carried out of the particle-level distributions from PYTHIA 8 simulations. Figure 4 shows the calculated pseudorapidity (η_{jet}) distribution of charged-particle jets recoiling from a high- p_T trigger hadron with TT{20,30} in MB and HM-selected event populations, for various lower thresholds in $p_{T,\text{jet}}^{\text{ch}}$. Since the per-trigger yield varies with $p_{T,\text{jet}}^{\text{ch}}$, these distributions are normalized to unit integral to enable a direct comparison of their shapes. The acceptances of V0A and V0C are also shown; note that V0C covers smaller values of $|\eta|$ than V0A. While the η_{jet} distribution for MB events is symmetric, the η_{jet} distribution for HM events is highly asymmetric, with significant enhancement in the relative rate of recoil jets in the V0C acceptance. The enhancement is largest for the highest value of $p_{T,\text{jet}}^{\text{ch}}$.

Figure 5 shows similar distributions for recoil jets with $p_{T,\text{jet}}^{\text{ch}} > 25$ GeV/c, in various intervals of V0M/⟨V0M⟩. A striking enhancement is observed in the per-trigger jet yield within the V0C acceptance for the largest values of V0M/⟨V0M⟩. Since HM events are selected based on the value of V0M/⟨V0M⟩, it is evident that the HM selection induces a bias which enhances the rate of hard recoil jets in the V0C acceptance.

Figure 6 provides additional insight into the bias induced by the HM event selection. The figure shows the probability to observe a specific number of jets with $R = 0.4$ and $p_{T,\text{jet}}^{\text{ch}} > 15$ GeV/c recoiling against a high- p_T hadron trigger (TT{20,30}) in the ALICE central barrel acceptance ($|\eta_{\text{jet}}| < 0.5$), for MB and HM pp collisions at $\sqrt{s} = 13$ TeV. Distributions are shown for both data and PYTHIA 8 calculations. In both data and simulations, the probability to observe a single jet is suppressed in HM relative to MB

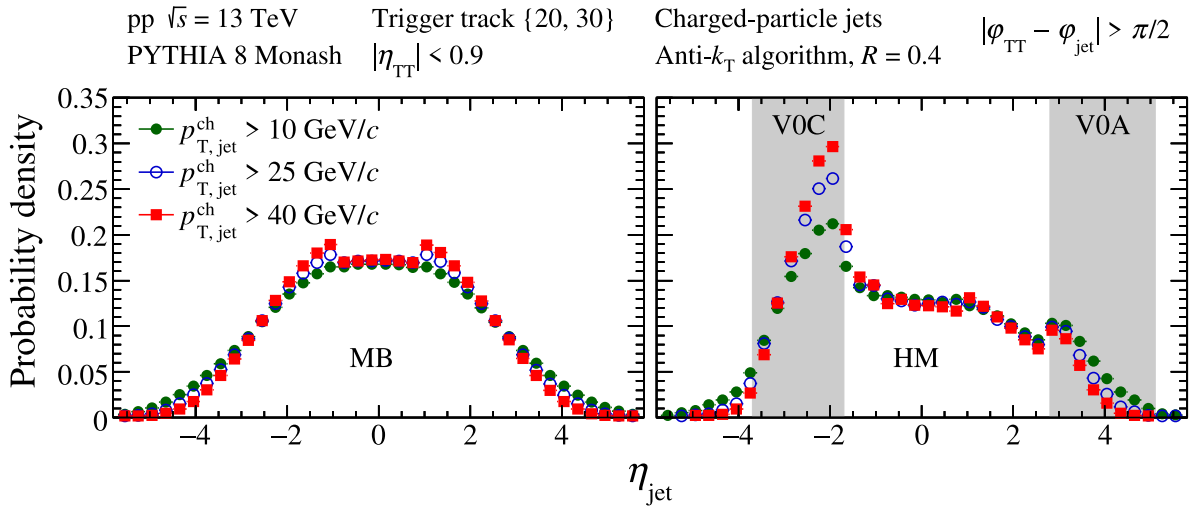


Figure 4: PYTHIA 8 particle-level simulation of the probability distribution of the yield of charged-particle jets ($R = 0.4$) recoiling from a high- p_{T} hadron (TT{20, 30}) as a function of η_{jet} for various $p_{\text{T, jet}}^{\text{ch}}$ intervals, in pp collisions at $\sqrt{s} = 13$ TeV. Left: MB events; right: HM events. VOA and VOC acceptances are also shown.

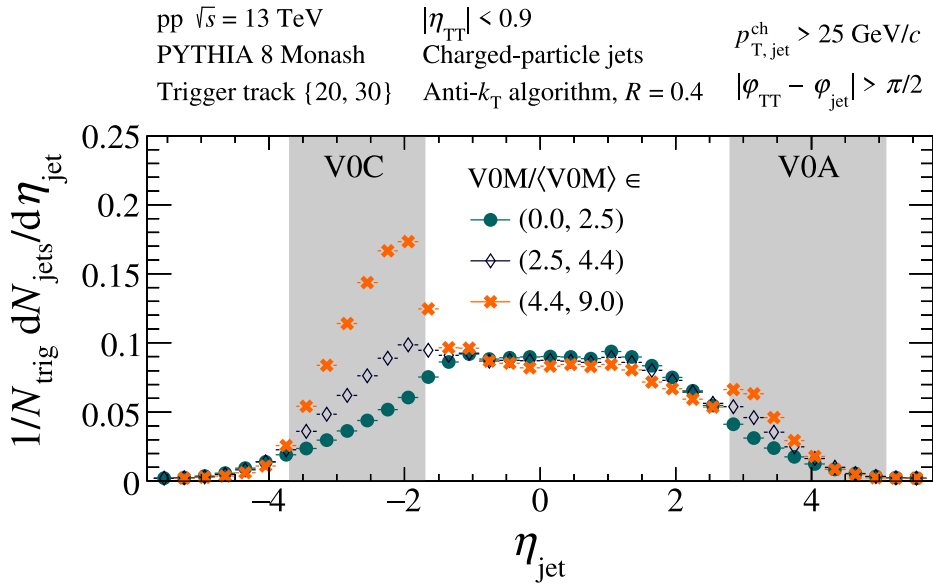


Figure 5: Same as Fig. 4, but for recoil jets with $p_{\text{T, jet}}^{\text{ch}} > 25$ GeV/c for various intervals in $VOM/\langle VOM \rangle$. Distributions are normalized per trigger.

events by 2–3%, while the probability to observe multiple jets is significantly enhanced.

The effect of the HM selection bias shown in Figs. 4, 5 and 6 on the acoplanarity distributions in Fig. 3 can be understood as follows. The HM requirement preferentially selects events with a recoil jet in the VOC acceptance. For the leading-order (LO) di-jet channel, in which the TT and recoil jet are azimuthally back-to-back, this depletes both the per-trigger rate for recoil jets observed in the central barrel ($|\eta_{\text{jet}}| < 0.9 - R$) at $\Delta\varphi \sim \pi$ and the relative rate of single recoil jets in the acceptance. The recoil jets observed in the ALICE central barrel in HM events therefore arise at enhanced rate from higher-order production processes, with multiple recoil jets in the final state. These jets from higher-order processes

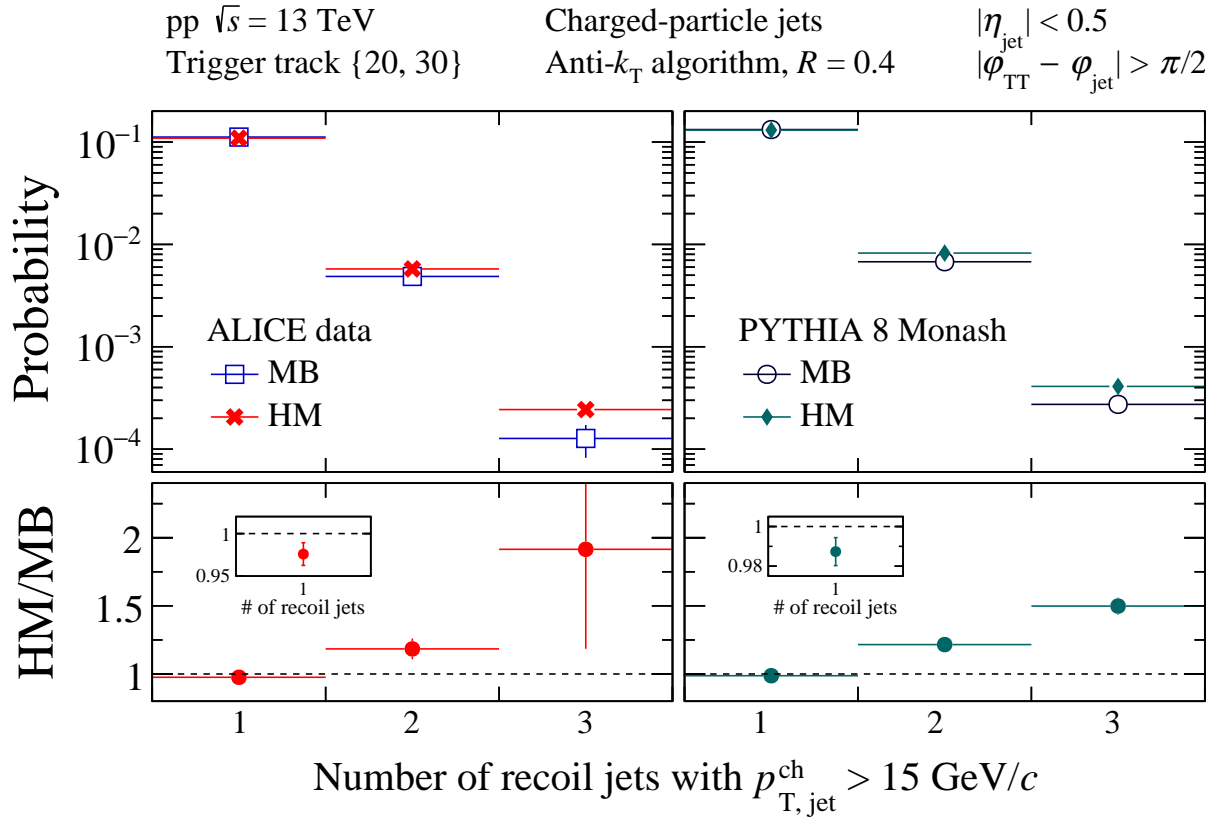


Figure 6: Distribution of probability per trigger hadron of number of jets with $R = 0.4$ and $p_{T, \text{jet}}^{\text{ch}} > 15$ GeV/ c recoiling from a high- p_T hadron (TT{20, 30}) at midrapidity ($|\eta_{\text{jet}}| < 0.5$), for MB and HM pp collisions at $\sqrt{s} = 13$ TeV. Left panels: ALICE data; right panels: simulations at the particle level with PYTHIA 8 Monash tune. Lower panels show the ratio HM/MB. The insert in the lower panels has magnified vertical scale to show the ratio of probabilities to observe a single jet.

have broader distribution in $\Delta\varphi$ than jets from LO production. This picture is confirmed by carrying out the PYTHIA 8 analysis for much larger recoil jet acceptance, $|\eta_{\text{jet}}| < 5.6$. In that case, no back-to-back yield depletion is observed.

The yield suppression and azimuthal broadening seen in Fig. 3 may therefore arise from the effect of different phase space being used for EA characterization (V0A and V0C) and recoil jet measurement (central barrel), combined with the HM selection bias towards events with a jet in the V0C acceptance. It therefore cannot be attributed uniquely to jet quenching in HM-selected events.

This conclusion about interpretability in terms of jet quenching of the effects seen in Fig. 3 is more general than this specific analysis, however. The bias of the HM event selection identified here is generic, and must also be taken into account for the interpretation in terms of QGP formation of other phenomena observed in small systems.

9 Summary

This article reports a search for jet quenching effects in high multiplicity pp collisions at $\sqrt{s} = 13$ TeV, based on the semi-inclusive azimuthal distribution of charged-particle jets recoiling from a high- p_T hadron trigger in the ALICE central barrel acceptance. Significant azimuthal broadening is observed in events selected to have high multiplicity in forward detectors, which may arise from jet quenching. However, similar broadening is also observed in simulations with the PYTHIA 8 event generator, which

does not incorporate jet quenching.

Detailed analysis of the data and simulations reveals that the high-multiplicity event selection, which is based on the V0 detectors at forward and backward rapidities, preferentially selects events with an energetic jet in the forward detector, consequently biasing the acoplanarity distribution measured in the central region. We conclude that this observable is therefore not uniquely sensitive to jet quenching effects in small collision systems. This bias is generic, however, and it should likewise be taken into account in the interpretation of other measurements which probe the formation of a quasi-equilibrated quark–gluon plasma in small collision systems.

Acknowledgements

The ALICE Collaboration would like to thank all its engineers and technicians for their invaluable contributions to the construction of the experiment and the CERN accelerator teams for the outstanding performance of the LHC complex. The ALICE Collaboration gratefully acknowledges the resources and support provided by all Grid centres and the Worldwide LHC Computing Grid (WLCG) collaboration. The ALICE Collaboration acknowledges the following funding agencies for their support in building and running the ALICE detector: A. I. Alikhanyan National Science Laboratory (Yerevan Physics Institute) Foundation (ANSL), State Committee of Science and World Federation of Scientists (WFS), Armenia; Austrian Academy of Sciences, Austrian Science Fund (FWF): [M 2467-N36] and Nationalstiftung für Forschung, Technologie und Entwicklung, Austria; Ministry of Communications and High Technologies, National Nuclear Research Center, Azerbaijan; Conselho Nacional de Desenvolvimento Científico e Tecnológico (CNPq), Financiadora de Estudos e Projetos (Finep), Fundação de Amparo à Pesquisa do Estado de São Paulo (FAPESP) and Universidade Federal do Rio Grande do Sul (UFRGS), Brazil; Bulgarian Ministry of Education and Science, within the National Roadmap for Research Infrastructures 2020–2027 (object CERN), Bulgaria; Ministry of Education of China (MOEC), Ministry of Science & Technology of China (MSTC) and National Natural Science Foundation of China (NSFC), China; Ministry of Science and Education and Croatian Science Foundation, Croatia; Centro de Aplicaciones Tecnológicas y Desarrollo Nuclear (CEADEN), Cubaenergía, Cuba; Ministry of Education, Youth and Sports of the Czech Republic, Czech Republic; The Danish Council for Independent Research | Natural Sciences, the VILLUM FONDEN and Danish National Research Foundation (DNRF), Denmark; Helsinki Institute of Physics (HIP), Finland; Commissariat à l’Energie Atomique (CEA) and Institut National de Physique Nucléaire et de Physique des Particules (IN2P3) and Centre National de la Recherche Scientifique (CNRS), France; Bundesministerium für Bildung und Forschung (BMBF) and GSI Helmholtzzentrum für Schwerionenforschung GmbH, Germany; General Secretariat for Research and Technology, Ministry of Education, Research and Religions, Greece; National Research, Development and Innovation Office, Hungary; Department of Atomic Energy Government of India (DAE), Department of Science and Technology, Government of India (DST), University Grants Commission, Government of India (UGC) and Council of Scientific and Industrial Research (CSIR), India; National Research and Innovation Agency - BRIN, Indonesia; Istituto Nazionale di Fisica Nucleare (INFN), Italy; Japanese Ministry of Education, Culture, Sports, Science and Technology (MEXT) and Japan Society for the Promotion of Science (JSPS) KAKENHI, Japan; Consejo Nacional de Ciencia (CONACYT) y Tecnología, through Fondo de Cooperación Internacional en Ciencia y Tecnología (FONCICYT) and Dirección General de Asuntos del Personal Académico (DGAPA), Mexico; Nederlandse Organisatie voor Wetenschappelijk Onderzoek (NWO), Netherlands; The Research Council of Norway, Norway; Commission on Science and Technology for Sustainable Development in the South (COMSATS), Pakistan; Pontificia Universidad Católica del Perú, Peru; Ministry of Education and Science, National Science Centre and WUT ID-UB, Poland; Korea Institute of Science and Technology Information and National Research Foundation of Korea (NRF), Republic of Korea; Ministry of Education and Scientific Research, Institute of Atomic Physics, Ministry of Research and Innovation and Institute of Atomic Physics and

University Politehnica of Bucharest, Romania; Ministry of Education, Science, Research and Sport of the Slovak Republic, Slovakia; National Research Foundation of South Africa, South Africa; Swedish Research Council (VR) and Knut & Alice Wallenberg Foundation (KAW), Sweden; European Organization for Nuclear Research, Switzerland; Suranaree University of Technology (SUT), National Science and Technology Development Agency (NSTDA), Thailand Science Research and Innovation (TSRI) and National Science, Research and Innovation Fund (NSRF), Thailand; Turkish Energy, Nuclear and Mineral Research Agency (TENMAK), Turkey; National Academy of Sciences of Ukraine, Ukraine; Science and Technology Facilities Council (STFC), United Kingdom; National Science Foundation of the United States of America (NSF) and United States Department of Energy, Office of Nuclear Physics (DOE NP), United States of America. In addition, individual groups or members have received support from: European Research Council, Strong 2020 - Horizon 2020 (grant nos. 950692, 824093), European Union; Academy of Finland (Center of Excellence in Quark Matter) (grant nos. 346327, 346328), Finland.

References

- [1] W. Busza, K. Rajagopal, and W. van der Schee, “Heavy Ion Collisions: The Big Picture, and the Big Questions”, *Ann. Rev. Nucl. Part. Sci.* **68** (2018) 339–376, arXiv:1802.04801 [hep-ph].
- [2] ALICE Collaboration, “The ALICE experiment – A journey through QCD”, arXiv:2211.04384 [nucl-ex].
- [3] U. Heinz and R. Snellings, “Collective flow and viscosity in relativistic heavy-ion collisions”, *Ann. Rev. Nucl. Part. Sci.* **63** (2013) 123–151, arXiv:1301.2826 [nucl-th].
- [4] ALICE Collaboration, J. Adam *et al.*, “Centrality dependence of particle production in p–Pb collisions at $\sqrt{s_{NN}} = 5.02$ TeV”, *Phys. Rev. C* **91** (2015) 064905, arXiv:1412.6828 [nucl-ex].
- [5] J. L. Nagle and W. A. Zajc, “Small System Collectivity in Relativistic Hadronic and Nuclear Collisions”, *Ann. Rev. Nucl. Part. Sci.* **68** (2018) 211–235, arXiv:1801.03477 [nucl-ex].
- [6] CMS Collaboration, V. Khachatryan *et al.*, “Observation of Long-Range Near-Side Angular Correlations in Proton-Proton Collisions at the LHC”, *JHEP* **1009** (2010) 091, arXiv:1009.4122 [nucl-ex].
- [7] ALICE Collaboration, B. Abelev *et al.*, “Long-range angular correlations on the near and away side in p–Pb collisions at $\sqrt{s_{NN}} = 5.02$ TeV”, *Phys. Lett. B* **719** (2013) 29–41, arXiv:1212.2001 [nucl-ex].
- [8] PHENIX Collaboration, C. Aidala *et al.*, “Creation of quark–gluon plasma droplets with three distinct geometries”, *Nature Phys.* **15** (2019) 214–220, arXiv:1805.02973 [nucl-ex].
- [9] STAR Collaboration, M. I. Abdulhamid *et al.*, “Measurements of the Elliptic and Triangular Azimuthal Anisotropies in Central $^3\text{He}+\text{Au}$, $\text{d}+\text{Au}$ and $\text{p}+\text{Au}$ Collisions at $\sqrt{s_{NN}} = 200$ GeV”, *Phys. Rev. Lett.* **130** (2023) 242301, arXiv:2210.11352 [nucl-ex].
- [10] ALICE Collaboration, J. Adam *et al.*, “Enhanced production of multi-strange hadrons in high-multiplicity proton–proton collisions”, *Nature Phys.* **13** (2017) 535–539, arXiv:1606.07424 [nucl-ex].
- [11] CMS Collaboration, V. Khachatryan *et al.*, “Measurement of the double-differential inclusive jet cross section in proton–proton collisions at $\sqrt{s} = 13$ TeV”, *Eur. Phys. J. C* **76** (2016) 451, arXiv:1605.04436 [hep-ex].
- [12] ATLAS Collaboration, M. Aaboud *et al.*, “Measurement of inclusive jet and dijet cross-sections in proton-proton collisions at $\sqrt{s} = 13$ TeV with the ATLAS detector”, *JHEP* **05** (2018) 195, arXiv:1711.02692 [hep-ex].
- [13] ALICE Collaboration, S. Acharya *et al.*, “Measurements of inclusive jet spectra in pp and central Pb–Pb collisions at $\sqrt{s_{NN}} = 5.02$ TeV”, *Phys. Rev. C* **101** (2020) 034911, arXiv:1909.09718 [nucl-ex].

- [14] A. Majumder and M. Van Leeuwen, “The Theory and Phenomenology of Perturbative QCD Based Jet Quenching”, *Prog. Part. Nucl. Phys. A* **66** (2011) 41–92, arXiv:1002.2206 [hep-ph].
- [15] L. Cunqueiro and A. M. Sickles, “Studying the QGP with Jets at the LHC and RHIC”, *Prog. Part. Nucl. Phys.* **124** (2022) 103940, arXiv:2110.14490 [nucl-ex].
- [16] X. Zhang and J. Liao, “Jet Quenching and Its Azimuthal Anisotropy in AA and possibly High Multiplicity pA and dA Collisions”, arXiv:1311.5463 [nucl-th].
- [17] K. Tywoniuk, “Is there jet quenching in pPb?”, *Nucl. Phys. A* **926** (2014) 85–91.
- [18] C. Park, C. Shen, S. Jeon, and C. Gale, “Rapidity-dependent jet energy loss in small systems with finite-size effects and running coupling”, *Nucl. Part. Phys. Proc.* **289–290** (2017) 289–292, arXiv:1612.06754 [nucl-th].
- [19] A. Huss, A. Kurkela, A. Mazeliauskas, R. Paatelainen, W. van der Schee, and U. A. Wiedemann, “Predicting parton energy loss in small collision systems”, *Phys. Rev. C* **103** (2021) 054903, arXiv:2007.13758 [hep-ph].
- [20] A. Huss, A. Kurkela, A. Mazeliauskas, R. Paatelainen, W. van der Schee, and U. A. Wiedemann, “Discovering Partonic Rescattering in Light Nucleus Collisions”, *Phys. Rev. Lett.* **126** (2021) 192301, arXiv:2007.13754 [hep-ph].
- [21] B. G. Zakharov, “Jet quenching from heavy to light ion collisions”, *JHEP* **09** (2021) 087, arXiv:2105.09350 [hep-ph].
- [22] W. Ke and I. Vitev, “Searching for QGP droplets with high- p_T hadrons and heavy flavor”, *Phys. Rev. C* **107** (2023) 064903, arXiv:2204.00634 [hep-ph].
- [23] M. L. Miller, K. Reygers, S. J. Sanders, and P. Steinberg, “Glauber modeling in high energy nuclear collisions”, *Ann. Rev. Nucl. Part. Sci.* **57** (2007) 205–243, arXiv:nucl-ex/0701025 [nucl-ex].
- [24] **PHENIX** Collaboration, A. Adare *et al.*, “Centrality-dependent modification of jet-production rates in deuteron-gold collisions at $\sqrt{s_{NN}} = 200$ GeV”, *Phys. Rev. Lett.* **116** (2016) 122301, arXiv:1509.04657 [nucl-ex].
- [25] **ATLAS** Collaboration, G. Aad *et al.*, “Centrality and rapidity dependence of inclusive jet production in $\sqrt{s_{NN}} = 5.02$ TeV proton-lead collisions with the ATLAS detector”, *Phys. Lett. B* **748** (2015) 392–413, arXiv:1412.4092 [hep-ex].
- [26] **PHENIX** Collaboration, A. Adare *et al.*, “Centrality categorization for $R_{p(d)+A}$ in high-energy collisions”, *Phys. Rev. C* **90** (2014) 034902, arXiv:1310.4793 [nucl-ex].
- [27] M. Alvioli, B. A. Cole, L. Frankfurt, D. V. Perepelitsa, and M. Strikman, “Evidence for x -dependent proton color fluctuations in pA collisions at the CERN Large Hadron Collider”, *Phys. Rev. C* **93** (2016) 011902, arXiv:1409.7381 [hep-ph].
- [28] A. Bzdak, V. Skokov, and S. Bathe, “Centrality dependence of high energy jets in p+Pb collisions at energies available at the CERN Large Hadron Collider”, *Phys. Rev. C* **93** (2016) 044901, arXiv:1408.3156 [hep-ph].
- [29] M. Kordell and A. Majumder, “Jets in d(p)-A Collisions: Color Transparency or Energy Conservation”, *Phys. Rev. C* **97** (2018) 054904, arXiv:1601.02595 [nucl-th].
- [30] C. Loizides and A. Morsch, “Absence of jet quenching in peripheral nucleus–nucleus collisions”, *Phys. Lett. B* **773** (2017) 408–411, arXiv:1705.08856 [nucl-ex].
- [31] M. Alvioli, L. Frankfurt, D. Perepelitsa, and M. Strikman, “Global analysis of color fluctuation effects in proton– and deuteron–nucleus collisions at RHIC and the LHC”, *Phys. Rev. D* **98** (2018) 071502, arXiv:1709.04993 [hep-ph].
- [32] **PHENIX** Collaboration, N. J. Abdulameer *et al.*, “Disentangling centrality bias and final-state effects in the production of high- p_T π^0 using direct γ in d–Au collisions at $\sqrt{s_{NN}} = 200$ GeV”, arXiv:2303.12899 [nucl-ex].

- [33] **ALICE** Collaboration, S. Acharya *et al.*, “Measurement of prompt D^0 , D^+ , D^{*+} , and D_S^+ production in p–Pb collisions at $\sqrt{s_{NN}} = 5.02$ TeV”, *JHEP* **12** (2019) 092, arXiv:1906.03425 [nucl-ex].
- [34] **ALICE** Collaboration, S. Acharya *et al.*, “Nuclear modification factor of light neutral-meson spectra up to high transverse momentum in p–Pb collisions at $\sqrt{s_{NN}} = 8.16$ TeV”, *Phys. Lett. B* **827** (2022) 136943, arXiv:2104.03116 [nucl-ex].
- [35] **ALICE** Collaboration, S. Acharya *et al.*, “Measurement of inclusive charged-particle b-jet production in pp and p–Pb collisions at $\sqrt{s_{NN}} = 5.02$ TeV”, *JHEP* **01** (2022) 178, arXiv:2110.06104 [nucl-ex].
- [36] **ALICE** Collaboration, S. Acharya *et al.*, “Constraints on jet quenching in p–Pb collisions at $\sqrt{s_{NN}} = 5.02$ TeV measured by the event-activity dependence of semi-inclusive hadron-jet distributions”, *Phys. Lett. B* **783** (2018) 95–113, arXiv:1712.05603 [nucl-ex].
- [37] **ATLAS** Collaboration, “Strong constraints on jet quenching in centrality-dependent p+Pb collisions at 5.02 TeV from ATLAS”, arXiv:2206.01138 [nucl-ex].
- [38] **ATLAS** Collaboration, G. Aad *et al.*, “Transverse momentum and process dependent azimuthal anisotropies in $\sqrt{s_{NN}} = 8.16$ TeV p+Pb collisions with the ATLAS detector”, *Eur. Phys. J. C* **80** (2020) 73, arXiv:1910.13978 [nucl-ex].
- [39] L. Yan and J.-Y. Ollitrault, “Universal fluctuation-driven eccentricities in proton-proton, proton-nucleus and nucleus-nucleus collisions”, *Phys. Rev. Lett.* **112** (2014) 082301, arXiv:1312.6555 [nucl-th].
- [40] C. Bierlich, G. Gustafson, and L. Lönnblad, “Collectivity without plasma in hadronic collisions”, *Phys. Lett. B* **779** (2018) 58–63, arXiv:1710.09725 [hep-ph].
- [41] B. Blok, C. D. Jäkel, M. Strikman, and U. A. Wiedemann, “Collectivity from interference”, *JHEP* **12** (2017) 074, arXiv:1708.08241 [hep-ph].
- [42] **ALICE** Collaboration, J. Adam *et al.*, “Measurement of jet quenching with semi-inclusive hadron-jet distributions in central Pb–Pb collisions at $\sqrt{s_{NN}} = 2.76$ TeV”, *JHEP* **09** (2015) 170, arXiv:1506.03984 [nucl-ex].
- [43] **STAR** Collaboration, L. Adamczyk *et al.*, “Measurements of jet quenching with semi-inclusive hadron+jet distributions in Au+Au collisions at $\sqrt{s_{NN}} = 200$ GeV”, *Phys. Rev. C* **96** (2017) 024905, arXiv:1702.01108 [nucl-ex].
- [44] M. Cacciari, G. P. Salam, and G. Soyez, “The anti- k_t jet clustering algorithm”, *JHEP* **04** (2008) 063, arXiv:0802.1189 [hep-ph].
- [45] D. A. Appel, “Jets as a Probe of Quark - Gluon Plasmas”, *Phys. Rev. D* **33** (1986) 717.
- [46] J. P. Blaizot and L. D. McLerran, “Jets in Expanding Quark - Gluon Plasmas”, *Phys. Rev. D* **34** (1986) 2739.
- [47] F. D’Eramo, H. Liu, and K. Rajagopal, “Transverse Momentum Broadening and the Jet Quenching Parameter, Redux”, *Phys. Rev. D* **84** (2011) 065015, arXiv:1006.1367 [hep-ph].
- [48] F. D’Eramo, M. Lekaveckas, H. Liu, and K. Rajagopal, “Momentum Broadening in Weakly Coupled Quark-Gluon Plasma (with a view to finding the quasiparticles within liquid quark-gluon plasma)”, *JHEP* **05** (2013) 031, arXiv:1211.1922 [hep-ph].
- [49] L. Chen, G.-Y. Qin, S.-Y. Wei, B.-W. Xiao, and H.-Z. Zhang, “Probing Transverse Momentum Broadening via Dihadron and Hadron-jet Angular Correlations in Relativistic Heavy-ion Collisions”, *Phys. Lett. B* **773** (2017) 672–676, arXiv:1607.01932 [hep-ph].
- [50] F. D’Eramo, K. Rajagopal, and Y. Yin, “Molière scattering in quark-gluon plasma: finding point-like scatterers in a liquid”, *JHEP* **01** (2019) 172, arXiv:1808.03250 [hep-ph].
- [51] **ALICE** Collaboration, K. Aamodt *et al.*, “The ALICE experiment at the CERN LHC”, *JINST* **3** (2008) S08002.

- [52] ALICE Collaboration, B. Abelev *et al.*, “Performance of the ALICE Experiment at the CERN LHC”, *Int. J. Mod. Phys. A* **29** (2014) 1430044, arXiv:1402.4476 [nucl-ex].
- [53] ALICE Collaboration, E. Abbas *et al.*, “Performance of the ALICE VZERO system”, *JINST* **8** (2013) P10016, arXiv:1306.3130 [nucl-ex].
- [54] ALICE Collaboration, S. Acharya *et al.*, “Measurement of charged jet cross section in pp collisions at $\sqrt{s} = 5.02$ TeV”, *Phys. Rev. D* **100** (2019) 092004, arXiv:1905.02536 [nucl-ex].
- [55] T. Sjöstrand, S. Mrenna, and P. Z. Skands, “A Brief Introduction to PYTHIA 8.1”, *Comput. Phys. Commun.* **178** (2008) 852–867, arXiv:hep-ph/0710.3820 [hep-ph].
- [56] P. Skands, S. Carrazza, and J. Rojo, “Tuning PYTHIA 8.1: the Monash 2013 Tune”, *Eur. Phys. J. C* **74** (2014) 3024, arXiv:1404.5630 [hep-ph].
- [57] R. Brun, F. Bruyant, M. Maire, A. C. McPherson, and P. Zancarini, *GEANT 3: user’s guide Geant 3.10, Geant 3.11; rev. version*. CERN, Geneva, 1987. <https://cds.cern.ch/record/1119728>.
- [58] ALICE Collaboration, P. Cortese *et al.*, *ALICE forward detectors: FMD, TO and VO: Technical Design Report*. 2004. <https://cds.cern.ch/record/781854>.
- [59] M. Cacciari, G. P. Salam, and G. Soyez, “FastJet User Manual”, *Eur. Phys. J. C* **72** (2012) 1896, arXiv:1111.6097 [hep-ph].
- [60] M. Cacciari and G. P. Salam, “Pileup subtraction using jet areas”, *Phys. Lett. B* **659** (2008) 119–126, arXiv:0707.1378 [hep-ph].
- [61] M. Cacciari, G. P. Salam, and G. Soyez, “The Catchment Area of Jets”, *JHEP* **04** (2008) 005, arXiv:0802.1188 [hep-ph].
- [62] ALICE Collaboration, S. Acharya *et al.*, “Multiplicity dependence of charged-particle jet production in pp collisions at $\sqrt{s} = 13$ TeV”, *Eur. Phys. J. C* **82** (2022) 514, arXiv:2202.01548 [nucl-ex].
- [63] D. de Florian, “Next-to-leading order QCD corrections to hadron+jet production in pp collisions at RHIC”, *Phys.Rev.* **D79** (2009) 114014, arXiv:0904.4402 [hep-ph].
- [64] ALICE Collaboration, S. Acharya *et al.*, “The ALICE definition of primary particles”, *ALICE-PUBLIC-2017-005* (2017). <https://cds.cern.ch/record/2270008>.
- [65] ALICE Collaboration, B. Abelev *et al.*, “Measurement of charged jet suppression in Pb–Pb collisions at $\sqrt{s_{NN}} = 2.76$ TeV”, *JHEP* **03** (2014) 013, arXiv:1311.0633 [nucl-ex].
- [66] G. D’Agostini, “Improved iterative Bayesian unfolding”, arXiv:1010.0632 [physics.data-an].
- [67] T. Adye, “Unfolding algorithms and tests using RooUnfold”, *CERN-2011-006* (2011) 313–318.
- [68] S. Frixione, P. Nason, and C. Oleari, “Matching NLO QCD computations with Parton Shower simulations: the POWHEG method”, *JHEP* **0711** (2007) 070, arXiv:0709.2092 [hep-ph].
- [69] S. Alioli, K. Hamilton, P. Nason, C. Oleari, and R. Emanuele, “Jet pair production in POWHEG”, *JHEP* **04** (2011) 081, arXiv:1012.3380 [hep-ph].
- [70] P. Sun, C. P. Yuan, and F. Yuan, “Soft Gluon Resummations in Dijet Azimuthal Angular Correlations in Hadronic Collisions”, *Phys. Rev. Lett.* **113** (2014) 232001, arXiv:1405.1105 [hep-ph].
- [71] P. Sun, C. P. Yuan, and F. Yuan, “Transverse Momentum Resummation for Dijet Correlation in Hadronic Collisions”, *Phys. Rev. D* **92** (2015) 094007, arXiv:1506.06170 [hep-ph].

A The ALICE Collaboration

S. Acharya ¹²⁶, D. Adamová ⁸⁶, G. Aglieri Rinella ³³, M. Agnello ³⁰, N. Agrawal ⁵¹, Z. Ahammed ¹³⁴, S. Ahmad ¹⁶, S.U. Ahn ⁷¹, I. Ahuja ³⁸, A. Akimov ¹⁴², M. Al-Turany ⁹⁷, D. Aleksandrov ¹⁴², B. Alessandro ⁵⁶, H.M. Alfanda ⁶, R. Alfaro Molina ⁶⁷, B. Ali ¹⁶, A. Alici ²⁶, N. Alizadehvandchali ¹¹⁵, A. Alkin ³³, J. Alme ²¹, G. Alocco ⁵², T. Alt ⁶⁴, A.R. Altamura ⁵⁰, I. Altsybeev ⁹⁵, M.N. Anaam ⁶, C. Andrei ⁴⁶, N. Andreou ¹¹⁴, A. Andronic ¹³⁷, V. Anguelov ⁹⁴, F. Antinori ⁵⁴, P. Antonioli ⁵¹, N. Apadula ⁷⁴, L. Aphecetche ¹⁰³, H. Appelshäuser ⁶⁴, C. Arata ⁷³, S. Arcelli ²⁶, M. Aresti ²³, R. Arnaldi ⁵⁶, J.G.M.C.A. Arneiro ¹¹⁰, I.C. Arsene ²⁰, M. Arslandok ¹³⁹, A. Augustinus ³³, R. Averbeck ⁹⁷, M.D. Azmi ¹⁶, H. Baba ¹²³, A. Badalà ⁵³, J. Bae ¹⁰⁴, Y.W. Baek ⁴¹, X. Bai ¹¹⁹, R. Bailhache ⁶⁴, Y. Bailung ⁴⁸, A. Balbino ³⁰, A. Baldisseri

¹²⁹, B. Balis ², D. Banerjee ⁴, Z. Banoo ⁹¹, R. Barbera ²⁷, F. Barile ³², L. Barioglio ⁹⁵, M. Barlou ⁷⁸, B. Barman ⁴², G.G. Barnaföldi ¹³⁸, L.S. Barnby ⁸⁵, V. Barret ¹²⁶, L. Barreto ¹¹⁰, C. Bartels ¹¹⁸, K. Barth ³³, E. Bartsch ⁶⁴, N. Bastid ¹²⁶, S. Basu ⁷⁵, G. Batigne ¹⁰³, D. Battistini ⁹⁵, B. Batyunya ¹⁴³, D. Bauri ⁴⁷, J.L. Bazo Alba ¹⁰¹, I.G. Bearden ⁸³, C. Beattie ¹³⁹, P. Becht ⁹⁷, D. Behera ⁴⁸, I. Belikov ¹²⁸, A.D.C. Bell Hechavarria ¹³⁷, F. Bellini ²⁶, R. Bellwied ¹¹⁵, S. Belokurova ¹⁴², Y.A.V. Beltran ⁴⁵, G. Bencedi ¹³⁸, S. Beole ²⁵, Y. Berdnikov ¹⁴², A. Berdnikova ⁹⁴, L. Bergmann ⁹⁴, M.G. Besoiu ⁶³, L. Betev ³³, P.P. Bhaduri ¹³⁴, A. Bhasin ⁹¹, M.A. Bhat ⁴, B. Bhattacharjee ⁴², L. Bianchi ²⁵, N. Bianchi ⁴⁹, J. Bielčik ³⁶, J. Bielčíková ⁸⁶, J. Biernat ¹⁰⁷, A.P. Bigot ¹²⁸, A. Bilandzic ⁹⁵, G. Biro ¹³⁸, S. Biswas ⁴, N. Bize

¹⁰³, J.T. Blair ¹⁰⁸, D. Blau ¹⁴², M.B. Blidaru ⁹⁷, N. Bluhme ³⁹, C. Blume ⁶⁴, G. Boca ^{22,55}, F. Bock ⁸⁷, T. Bodova ²¹, A. Bogdanov ¹⁴², S. Boi ²³, J. Bok ⁵⁸, L. Boldizsár ¹³⁸, M. Bombara ³⁸, P.M. Bond ³³, G. Bonomi ^{133,55}, H. Borel ¹²⁹, A. Borissov ¹⁴², A.G. Borquez Carcamo ⁹⁴, H. Bossi ¹³⁹, E. Botta ²⁵, Y.E.M. Bouziani ⁶⁴, L. Bratrud ⁶⁴, P. Braun-Munzinger ⁹⁷, M. Bregant ¹¹⁰, M. Broz ³⁶, G.E. Bruno ^{96,32}, M.D. Buckland ²⁴, D. Budnikov ¹⁴², H. Buesching ⁶⁴, S. Bufalino ³⁰, P. Buhler ¹⁰², N. Burmasov ¹⁴², Z. Buthelezi ^{68,122}, A. Bylinkin ²¹, S.A. Bysiak ¹⁰⁷, M. Cai ⁶, H. Caines ¹³⁹, A. Caliva ²⁹, E. Calvo Villar ¹⁰¹, J.M.M. Camacho ¹⁰⁹, P. Camerini ²⁴, F.D.M. Canedo ¹¹⁰, M. Carabas ¹²⁵, A.A. Carballo ³³, F. Carnesecchi ³³, R. Caron ¹²⁷, L.A.D. Carvalho ¹¹⁰, J. Castillo Castellanos ¹²⁹, F. Catalano ^{33,25}, C. Ceballos Sanchez ¹⁴³, I. Chakaberia ⁷⁴, P. Chakraborty ⁴⁷, S.
Chandra ¹³⁴, S. Chapeland ³³, M. Chartier ¹¹⁸, S. Chattopadhyay ¹³⁴, S. Chattopadhyay ⁹⁹, T.G. Chavez ⁴⁵, T. Cheng ^{97,6}, C. Cheshkov ¹²⁷, B. Cheynis ¹²⁷, V. Chibante Barroso ³³, D.D. Chinellato ¹¹¹, E.S. Chizzali ^{1,95}, J. Cho ⁵⁸, S. Cho ⁵⁸, P. Chochula ³³, D. Choudhury ⁴², P. Christakoglou ⁸⁴, C.H. Christensen ⁸³, P. Christiansen ⁷⁵, T. Chujo ¹²⁴, M. Ciacco ³⁰, C. Cicalo ⁵², F. Cindolo ⁵¹, M.R. Ciupek ⁹⁷, G. Clai ^{II,51}, F. Colamaria ⁵⁰, J.S. Colburn ¹⁰⁰, D. Colella ^{96,32}, M. Colocci ²⁶, M. Concas ^{III,33}, G. Conesa Balbastre ⁷³, Z. Conesa del Valle ¹³⁰, G. Contin ²⁴, J.G. Contreras ³⁶, M.L. Coquet ¹²⁹, P. Cortese ^{132,56}, M.R. Cosentino ¹¹², F. Costa ³³, S. Costanza ^{22,55}, C. Cot ¹³⁰, J. Crkovská ⁹⁴, P. Crochet ¹²⁶, R. Cruz-Torres ⁷⁴, P. Cui ⁶, A. Dainese ⁵⁴, M.C. Danisch ⁹⁴, A. Danu ⁶³, P. Das ⁸⁰, P. Das ⁴, S. Das ⁴, A.R. Dash ¹³⁷, S. Dash ⁴⁷, R.M.H. David

⁴⁵, A. De Caro ²⁹, G. de Cataldo ⁵⁰, J. de Cuveland ³⁹, A. De Falco ²³, D. De Gruttola ²⁹, N. De Marco ⁵⁶, C. De Martin ²⁴, S. De Pasquale ²⁹, R. Deb ¹³³, R. Del Grande ⁹⁵, L. Dello Stritto ²⁹, W. Deng ⁶, P. Dhankher ¹⁹, D. Di Bari ³², A. Di Mauro ³³, B. Diab ¹²⁹, R.A. Diaz ^{143,7}, T. Dietel ¹¹³, Y. Ding ⁶, J. Ditzel ⁶⁴, R. Divià ³³, D.U. Dixit ¹⁹, Ø. Djuvsland ²¹, U. Dmitrieva ¹⁴², A. Dobrin ⁶³, B. Dönigus ⁶⁴, J.M. Dubinski ¹³⁵, A. Dubla ⁹⁷, S. Dudi ⁹⁰, P. Dupieux ¹²⁶, M. Durkac ¹⁰⁶, N. Dzalaiova ¹³, T.M. Eder ¹³⁷, R.J. Ehlers ⁷⁴, F. Eisenhut ⁶⁴, R. Ejima ⁹², D. Elia ⁵⁰, B. Erazmus ¹⁰³, F. Ercolessi ²⁶, B. Espagnon ¹³⁰, G. Eulisse ³³, D. Evans ¹⁰⁰, S. Evdokimov ¹⁴², L. Fabbietti ⁹⁵, M. Faggin ²⁸, J. Faivre ⁷³, F. Fan ⁶, W. Fan ⁷⁴, A. Fantoni ⁴⁹, M. Fasel ⁸⁷, P. Fecchio ³⁰, A. Feliciello ⁵⁶, G. Feofilov

¹⁴², A. Fernández Téllez ⁴⁵, L. Ferrandi ¹¹⁰, M.B. Ferrer ³³, A. Ferrero ¹²⁹, C. Ferrero ⁵⁶, A. Ferretti ²⁵, V.J.G. Feuillard ⁹⁴, V. Filova ³⁶, D. Finogeev ¹⁴², F.M. Fionda ⁵², E. Flatland ³³, F. Flor ¹¹⁵, A.N. Flores ¹⁰⁸, S. Foertsch ⁶⁸, I. Fokin ⁹⁴, S. Fokin ¹⁴², E. Fragiaco ⁵⁷, E. Frajna ¹³⁸, U. Fuchs ³³, N. Funicello ²⁹, C. Furget ⁷³, A. Furs ¹⁴², T. Fusayasu ⁹⁸, J.J. Gaardhøje ⁸³, M. Gagliardi ²⁵, A.M. Gago ¹⁰¹, T. Gahlaut ⁴⁷, C.D. Galvan ¹⁰⁹, D.R. Gangadharan ¹¹⁵, P. Ganoti ⁷⁸, C. Garabatos ⁹⁷, A.T. Garcia ¹³⁰, J.R.A. Garcia ⁴⁵, E. Garcia-Solis ⁹, C. Gargiulo ³³, P. Gasik ⁹⁷, A. Gautam ¹¹⁷, M.B. Gay Ducati ⁶⁶, M. Germain ¹⁰³, A. Ghimouz ¹²⁴, C. Ghosh

W. Guo⁶, A. Gupta⁹¹, R. Gupta⁹¹, R. Gupta⁴⁸, S.P. Guzman⁴⁵, K. Gwizdzial¹³⁵, L. Gyulai¹³⁸, C. Hadjidakis¹³⁰, F.U. Haider⁹¹, S. Haidlova³⁶, H. Hamagaki⁷⁶, A. Hamdi⁷⁴, Y. Han¹⁴⁰, B.G. Hanley¹³⁶, R. Hannigan¹⁰⁸, J. Hansen⁷⁵, M.R. Haque¹³⁵, J.W. Harris¹³⁹, A. Harton⁹, H. Hassan¹¹⁶, D. Hatzifotiadou⁵¹, P. Hauer⁴³, L.B. Havener¹³⁹, S.T. Heckel⁹⁵, E. Hellbär⁹⁷, H. Helstrup³⁵, M. Hemmer⁶⁴, T. Herman³⁶, G. Herrera Corral⁸, F. Herrmann¹³⁷, S. Herrmann¹²⁷, K.F. Hetland³⁵, B. Heybeck⁶⁴, H. Hillemanns³³, B. Hippolyte¹²⁸, F.W. Hoffmann⁷⁰, B. Hofman⁵⁹, G.H. Hong¹⁴⁰, M. Horst⁹⁵, A. Horzyk², Y. Hou⁶, P. Hristov³³, C. Hughes¹²¹, P. Huhn⁶⁴, L.M. Huhta¹¹⁶, T.J. Humanic⁸⁸, A. Hutson¹¹⁵, D. Hutter³⁹, R. Ilkaev¹⁴², H. Ilyas¹⁴, M. Inaba¹²⁴, G.M. Innocenti³³, M. Ippolitov¹⁴², A. Isakov^{84,86}, T. Isidori¹¹⁷, M.S. Islam⁹⁹, M. Ivanov⁹⁷, M. Ivanov¹³, V. Ivanov¹⁴², K.E. Iversen⁷⁵, M. Jablonski², B. Jacak⁷⁴, N. Jacazio²⁶, P.M. Jacobs⁷⁴, S. Jadlovská¹⁰⁶, J. Jadlovsky¹⁰⁶, S. Jaelani⁸², C. Jahnke¹¹⁰, M.J. Jakubowska¹³⁵, M.A. Janik¹³⁵, T. Janson⁷⁰, S. Ji¹⁷, S. Jia¹⁰, A.A.P. Jimenez⁶⁵, F. Jonas⁸⁷, D.M. Jones¹¹⁸, J.M. Jowett^{33,97}, J. Jung⁶⁴, M. Jung⁶⁴, A. Junique³³, A. Jusko¹⁰⁰, M.J. Kabus^{33,135}, J. Kaewjai¹⁰⁵, P. Kalinak⁶⁰, A.S. Kalteyer⁹⁷, A. Kalweit³³, V. Kaplin¹⁴², A. Karasu Uysal⁷², D. Karatovic⁸⁹, O. Karavichev¹⁴², T. Karavicheva¹⁴², P. Karczmarczyk¹³⁵, E. Karpechev¹⁴², U. Kebschull⁷⁰, R. Keidel¹⁴¹, D.L.D. Keijndener⁵⁹, M. Keil³³, B. Ketzer⁴³, S.S. Khade⁴⁸, A.M. Khan¹¹⁹, S. Khan¹⁶, A. Khanzadeev¹⁴², Y. Kharlov¹⁴², A. Khatun¹¹⁷, A. Khuntia³⁶, B. Kileng³⁵, B. Kim¹⁰⁴, C. Kim¹⁷, D.J. Kim¹¹⁶, E.J. Kim⁶⁹, J. Kim¹⁴⁰, J.S. Kim⁴¹, J. Kim⁵⁸, J. Kim⁶⁹, M. Kim¹⁹, S. Kim¹⁸, T. Kim¹⁴⁰, K. Kimura⁹², S. Kirsch⁶⁴, I. Kisel³⁹, S. Kiselev¹⁴², A. Kisiel¹³⁵, J.P. Kitowski², J.L. Klay⁵, J. Klein³³, S. Klein⁷⁴, C. Klein-Bösing¹³⁷, M. Kleiner⁶⁴, T. Klemenz⁹⁵, A. Kluge³³, A.G. Knospe¹¹⁵, C. Kobdaj¹⁰⁵, T. Kollegger⁹⁷, A. Kondratyev¹⁴³, N. Kondratyeva¹⁴², E. Kondratyuk¹⁴², J. König⁶⁴, S.A. Königstorfer⁹⁵, P.J. Konopka³³, G. Kornakov¹³⁵, S.D. Koryciak², A. Kotliarov^{86,36}, V. Kovalenko¹⁴², M. Kowalski¹⁰⁷, V. Kozuharov³⁷, I. Králik⁶⁰, A. Kravčáková³⁸, L. Krcal^{33,39}, M. Krivda^{100,60}, F. Krizek⁸⁶, K. Krizkova Gajdosova³³, M. Kroesen⁹⁴, M. Krüger⁶⁴, D.M. Krupova³⁶, E. Kryshen¹⁴², V. Kučera⁵⁸, C. Kuhn¹²⁸, P.G. Kuijter⁸⁴, T. Kumaoka¹²⁴, D. Kumar¹³⁴, L. Kumar⁹⁰, N. Kumar⁹⁰, S. Kumar³², S. Kundu³³, P. Kurashvili⁷⁹, A. Kurepin¹⁴², A.B. Kurepin¹⁴², A. Kuryakin¹⁴², S. Kushpil⁸⁶, M.J. Kweon⁵⁸, Y. Kwon¹⁴⁰, S.L. La Pointe³⁹, P. La Rocca²⁷, A. Lakrathok¹⁰⁵, M. Lamanna³³, R. Langoy¹²⁰, P. Larionov³³, E. Laudi³³, L. Lautner^{33,95}, R. Lavicka¹⁰², R. Lea^{133,55}, H. Lee¹⁰⁴, I. Legrand⁴⁶, G. Legras¹³⁷, J. Lehrbach³⁹, T.M. Lelek², R.C. Lemmon⁸⁵, I. León Monzón¹⁰⁹, M.M. Lesch⁹⁵, E.D. Lesser¹⁹, P. Lévai¹³⁸, X. Li¹⁰, J. Lien¹²⁰, R. Lietava¹⁰⁰, I. Likmeta¹¹⁵, B. Lim²⁵, S.H. Lim¹⁷, V. Lindenstruth³⁹, A. Lindner⁴⁶, C. Lippmann⁹⁷, D.H. Liu⁶, J. Liu¹¹⁸, G.S.S. Liveraro¹¹¹, I.M. Lofnes²¹, C. Loizides⁸⁷, S. Lokos¹⁰⁷, J. Lomker⁵⁹, P. Loncar³⁴, X. Lopez¹²⁶, E. López Torres⁷, P. Lu^{97,119}, F.V. Lugo⁶⁷, J.R. Luhder¹³⁷, M. Lunardon²⁸, G. Luparello⁵⁷, Y.G. Ma⁴⁰, M. Mager³³, A. Maire¹²⁸, M.V. Makariev³⁷, M. Malaev¹⁴², G. Malfattore²⁶, N.M. Malik⁹¹, Q.W. Malik²⁰, S.K. Malik⁹¹, L. Malinina^{VI,143}, D. Mallick^{130,80}, N. Mallick⁴⁸, G. Mandaglio^{31,53}, S.K. Mandal⁷⁹, V. Manko¹⁴², F. Manso¹²⁶, V. Manzari⁵⁰, Y. Mao⁶, R.W. Marcjan², G.V. Margagliotti²⁴, A. Margotti⁵¹, A. Marín⁹⁷, C. Markert¹⁰⁸, P. Martinengo³³, M.I. Martínez⁴⁵, G. Martínez García¹⁰³, M.P.P. Martins¹¹⁰, S. Masciocchi⁹⁷, M. Masera²⁵, A. Masoni⁵², L. Massacrier¹³⁰, O. Massen⁵⁹, A. Mastroserio^{131,50}, O. Matonoha⁷⁵, S. Mattiazzo²⁸, A. Matyja¹⁰⁷, C. Mayer¹⁰⁷, A.L. Mazuecos³³, F. Mazzaschi²⁵, M. Mazzilli³³, J.E. Mdhluli¹²², Y. Melikyan⁴⁴, A. Menchaca-Rocha⁶⁷, J.E.M. Mendez⁶⁵, E. Meninno^{102,29}, A.S. Menon¹¹⁵, M. Meres¹³, S. Mhlanga^{113,68}, Y. Miake¹²⁴, L. Micheletti³³, D.L. Mihaylov⁹⁵, K. Mikhaylov^{143,142}, A.N. Mishra¹³⁸, D. Miśkowiec⁹⁷, A. Modak⁴, B. Mohanty⁸⁰, M. Mohisin Khan^{IV,16}, M.A. Molander⁴⁴, S. Monira¹³⁵, C. Mordasini¹¹⁶, D.A. Moreira De Godoy¹³⁷, I. Morozov¹⁴², A. Morsch³³, T. Mrnjavac³³, V. Muccifora⁴⁹, S. Muhuri¹³⁴, J.D. Mulligan⁷⁴, A. Mulliri²³, M.G. Munhoz¹¹⁰, R.H. Munzer⁶⁴, H. Murakami¹²³, S. Murray¹¹³, L. Musa³³, J. Musinsky⁶⁰, J.W. Myrcha¹³⁵, B. Naik¹²², A.I. Nambrath¹⁹, B.K. Nandi⁴⁷, R. Nania⁵¹, E. Nappi⁵⁰, A.F. Nassirpour¹⁸, A. Nath⁹⁴, C. Nattrass¹²¹, M.N. Naydenov³⁷, A. Neagu²⁰, A. Negru¹²⁵, L. Nellen⁶⁵, R. Nepeivoda⁷⁵, S. Nese²⁰, G. Neskovic³⁹, N. Nicassio⁵⁰, B.S. Nielsen⁸³, E.G. Nielsen⁸³, S. Nikolaev¹⁴², S. Nikulin¹⁴², V. Nikulin¹⁴², F. Noferini⁵¹, S. Noh¹², P. Nomokonov¹⁴³, J. Norman¹¹⁸, N. Novitzky⁸⁷, P. Nowakowski¹³⁵, A. Nyanin¹⁴², J. Nystrand²¹, M. Ogino⁷⁶, S. Oh¹⁸, A. Ohlson⁷⁵, V.A. Okorokov¹⁴², J. Oleniacz¹³⁵, A.C. Oliveira Da Silva¹²¹, A. Onnerstad¹¹⁶, C. Oppedisano⁵⁶, A. Ortiz Velasquez⁶⁵, J. Otwinowski¹⁰⁷, M. Oya⁹², K. Oyama⁷⁶, Y. Pachmayer⁹⁴, S. Padhan⁴⁷, D. Pagano^{133,55}, G. Paic⁶⁵, A. Palasciano⁵⁰, S. Panebianco¹²⁹, H. Park¹²⁴, H. Park¹⁰⁴, J. Park⁵⁸, J.E. Parkkila³³, Y. Patley⁴⁷, R.N. Patra⁹¹,

B. Paul²³, H. Pei⁶, T. Peitzmann⁵⁹, X. Peng¹¹, M. Pennisi²⁵, S. Perciballi²⁵, D. Peresunko¹⁴²,
 G.M. Perez⁷, Y. Pestov¹⁴², V. Petrov¹⁴², M. Petrovici⁴⁶, R.P. Pezzi^{103,66}, S. Piano⁵⁷, M. Pikna¹³,
 P. Pillot¹⁰³, O. Pinazza^{51,33}, L. Pinsky¹¹⁵, C. Pinto⁹⁵, S. Pisano⁴⁹, M. Płoskoń⁷⁴, M. Planinic⁸⁹,
 F. Pliquet⁶⁴, M.G. Poghosyan⁸⁷, B. Polichtchouk¹⁴², S. Politano³⁰, N. Poljak⁸⁹, A. Pop⁴⁶,
 S. Porteboeuf-Houssais¹²⁶, V. Pozdniakov¹⁴³, I.Y. Pozos⁴⁵, K.K. Pradhan⁴⁸, S.K. Prasad⁴,
 S. Prasad⁴⁸, R. Preghenella⁵¹, F. Prino⁵⁶, C.A. Pruneau¹³⁶, I. Pshenichnov¹⁴², M. Puccio³³,
 S. Pucillo²⁵, Z. Pugelova¹⁰⁶, S. Qiu⁸⁴, L. Quaglia²⁵, S. Ragoni¹⁵, A. Rai¹³⁹,
 A. Rakotozafindrabe¹²⁹, L. Ramello^{132,56}, F. Rami¹²⁸, S.A.R. Ramirez⁴⁵, T.A. Rancien⁷³, M. Rasa²⁷,
 S.S. Räsänen⁴⁴, R. Rath⁵¹, M.P. Rauch²¹, I. Ravasenga⁸⁴, K.F. Read^{87,121}, C. Reckziegel¹¹²,
 A.R. Redelbach³⁹, K. Redlich^{V,79}, C.A. Reetz⁹⁷, A. Rehman²¹, F. Reidt³³, H.A. Reme-Ness³⁵,
 Z. Rescakova³⁸, K. Reygers⁹⁴, A. Riabov¹⁴², V. Riabov¹⁴², R. Ricci²⁹, M. Richter²⁰,
 A.A. Riedel⁹⁵, W. Riegler³³, A.G. Riffero²⁵, C. Ristea⁶³, M.V. Rodriguez³³, M. Rodríguez
 Cahuantzi⁴⁵, K. Røed²⁰, R. Rogalev¹⁴², E. Rogochaya¹⁴³, T.S. Rogoschinski⁶⁴, D. Rohr³³,
 D. Röhrich²¹, P.F. Rojas⁴⁵, S. Rojas Torres³⁶, P.S. Rokita¹³⁵, G. Romanenko²⁶, F. Ronchetti⁴⁹,
 A. Rosano^{31,53}, E.D. Rosas⁶⁵, K. Roslon¹³⁵, A. Rossi⁵⁴, A. Roy⁴⁸, S. Roy⁴⁷, N. Rubini²⁶,
 D. Ruggiano¹³⁵, R. Rui²⁴, P.G. Russek², R. Russo⁸⁴, A. Rustamov⁸¹, E. Ryabinkin¹⁴²,
 Y. Ryabov¹⁴², A. Rybicki¹⁰⁷, H. Rytönen¹¹⁶, J. Ryu¹⁷, W. Rzesza¹³⁵, O.A.M. Saariimaki⁴⁴,
 S. Sadhu³², S. Sadovsky¹⁴², J. Saetre²¹, K. Šafařík³⁶, P. Saha⁴², S.K. Saha⁴, S. Saha⁸⁰,
 B. Sahoo⁴⁷, B. Sahoo⁴⁸, R. Sahoo⁴⁸, S. Sahoo⁶¹, D. Sahu⁴⁸, P.K. Sahu⁶¹, J. Saini¹³⁴,
 K. Sajdakova³⁸, S. Sakai¹²⁴, M.P. Salvan⁹⁷, S. Sambyal⁹¹, D. Samitz¹⁰², I. Sanna^{33,95},
 T.B. Saramela¹¹⁰, P. Sarma⁴², V. Sarritzu²³, V.M. Sarti⁹⁵, M.H.P. Sas³³, S. Sawan⁸⁰, J. Schambach⁸⁷,
 H.S. Scheid⁶⁴, C. Schiaua⁴⁶, R. Schicker⁹⁴, F. Schlepfer⁹⁴, A. Schmah⁹⁷, C. Schmidt⁹⁷,
 H.R. Schmidt⁹³, M.O. Schmidt³³, M. Schmidt⁹³, N.V. Schmidt⁸⁷, A.R. Schmier¹²¹, R. Schotter¹²⁸,
 A. Schröter³⁹, J. Schukraft³³, K. Schweda⁹⁷, G. Scioli²⁶, E. Scomparin⁵⁶, J.E. Seger¹⁵,
 Y. Sekiguchi¹²³, D. Sekihata¹²³, M. Selina⁸⁴, I. Selyuzhenkov⁹⁷, S. Senyukov¹²⁸, J.J. Seo^{94,58},
 D. Serebryakov¹⁴², L. Šerkšnytė⁹⁵, A. Sevcenco⁶³, T.J. Shaba⁶⁸, A. Shabetai¹⁰³, R. Shahoyan³³,
 A. Shangaraev¹⁴², A. Sharma⁹⁰, B. Sharma⁹¹, D. Sharma⁴⁷, H. Sharma^{54,107}, M. Sharma⁹¹,
 S. Sharma⁷⁶, S. Sharma⁹¹, U. Sharma⁹¹, A. Shatat¹³⁰, O. Sheibani¹¹⁵, K. Shigaki⁹²,
 M. Shimomura⁷⁷, J. Shin¹², S. Shirinkin¹⁴², Q. Shou⁴⁰, Y. Sibirak¹⁴², S. Siddhanta⁵²,
 T. Siemiarczuk⁷⁹, T.F. Silva¹¹⁰, D. Silvermyr⁷⁵, T. Simantathammakul¹⁰⁵, R. Simeonov³⁷, B. Singh⁹¹,
 B. Singh⁹⁵, K. Singh⁴⁸, R. Singh⁸⁰, R. Singh⁹¹, R. Singh⁴⁸, S. Singh¹⁶, V.K. Singh¹³⁴,
 V. Singhal¹³⁴, T. Sinha⁹⁹, B. Sitar¹³, M. Sitta^{132,56}, T.B. Skaali²⁰, G. Skorodumovs⁹⁴,
 M. Slupecki⁴⁴, N. Smirnov¹³⁹, R.J.M. Snellings⁵⁹, E.H. Solheim²⁰, J. Song¹⁷, C. Sonnabend^{33,97},
 F. Soramel²⁸, A.B. Soto-hernandez⁸⁸, R. Spijkers⁸⁴, I. Sputowska¹⁰⁷, J. Staa⁷⁵, J. Stachel⁹⁴,
 I. Stan⁶³, P.J. Steffanic¹²¹, S.F. Stiefelmaier⁹⁴, D. Stocco¹⁰³, I. Storehaug²⁰, P. Stratmann¹³⁷,
 S. Strazzi²⁶, A. Sturniolo^{31,53}, C.P. Stylianidis⁸⁴, A.A.P. Suaide¹¹⁰, C. Suire¹³⁰, M. Sukhanov¹⁴²,
 M. Suljic³³, R. Sultanov¹⁴², V. Sumberia⁹¹, S. Sumowidagdo⁸², S. Swain⁶¹, I. Szarka¹³,
 M. Szymkowski¹³⁵, S.F. Taghavi⁹⁵, G. Taillepied⁹⁷, J. Takahashi¹¹¹, G.J. Tambave⁸⁰, S. Tang⁶,
 Z. Tang¹¹⁹, J.D. Tapia Takaki¹¹⁷, N. Tapus¹²⁵, L.A. Tarasovicova¹³⁷, M.G. Tarzila⁴⁶, G.F. Tassielli³²,
 A. Tauro³³, G. Tejeda Muñoz⁴⁵, A. Telesca³³, L. Terlizzi²⁵, C. Terrevoli¹¹⁵, S. Thakur⁴,
 D. Thomas¹⁰⁸, A. Tikhonov¹⁴², N. Tiltmann^{33,137}, A.R. Timmins¹¹⁵, M. Tkacik¹⁰⁶, T. Tkacik¹⁰⁶,
 A. Toia⁶⁴, R. Tokumoto⁹², K. Tomohiro⁹², N. Topilskaya¹⁴², M. Toppi⁴⁹, T. Tork¹³⁰, P.V. Torres⁶⁵,
 V.V. Torres¹⁰³, A.G. Torres Ramos³², A. Trifiro^{31,53}, A.S. Triolo^{33,31,53}, S. Tripathy⁵¹,
 T. Tripathy⁴⁷, S. Trogolo³³, V. Trubnikov³, W.H. Trzaska¹¹⁶, T.P. Trzcinski¹³⁵, A. Tumkin¹⁴²,
 R. Turrisi⁵⁴, T.S. Tveter²⁰, K. Ullaland²¹, B. Ulukutlu⁹⁵, A. Uras¹²⁷, G.L. Usai²³, M. Vala³⁸,
 N. Valle²², L.V.R. van Doremalen⁵⁹, M. van Leeuwen⁸⁴, C.A. van Veen⁹⁴, R.J.G. van Weelden⁸⁴,
 P. Vande Vyvre³³, D. Varga¹³⁸, Z. Varga¹³⁸, M. Vasileiou⁷⁸, A. Vasiliev¹⁴², O. Vázquez Doce⁴⁹,
 O. Vazquez Rueda¹¹⁵, V. Vechernin¹⁴², E. Vercellin²⁵, S. Vergara Limón⁴⁵, R. Verma⁴⁷, L. Vermunt⁹⁷,
 R. Vértesi¹³⁸, M. Verweij⁵⁹, L. Vickovic³⁴, Z. Vilakazi¹²², O. Villalobos Baillie¹⁰⁰, A. Villani²⁴,
 A. Vinogradov¹⁴², T. Virgili²⁹, M.M.O. Virta¹¹⁶, V. Vislavicius⁷⁵, A. Vodopyanov¹⁴³, B. Volkel³³,
 M.A. Völkl⁹⁴, K. Voloshin¹⁴², S.A. Voloshin¹³⁶, G. Volpe³², B. von Haller³³, I. Vorobyev⁹⁵,
 N. Vozniuk¹⁴², J. Vrláková³⁸, J. Wan⁴⁰, C. Wang⁴⁰, D. Wang⁴⁰, Y. Wang⁴⁰, Y. Wang⁶,
 A. Wegrzynek³³, F.T. Weiglhofer³⁹, S.C. Wenzel³³, J.P. Wessels¹³⁷, S.L. Weyhmiller¹³⁹,
 J. Wiechula⁶⁴, J. Wikne²⁰, G. Wilk⁷⁹, J. Wilkinson⁹⁷, G.A. Willems¹³⁷, B. Windelband⁹⁴,
 M. Winn¹²⁹, J.R. Wright¹⁰⁸, W. Wu⁴⁰, Y. Wu¹¹⁹, R. Xu⁶, A. Yadav⁴³, A.K. Yadav¹³⁴,
 S. Yalcin⁷², Y. Yamaguchi⁹², S. Yang²¹, S. Yano⁹², Z. Yin⁶, I.-K. Yoo¹⁷, J.H. Yoon⁵⁸, H. Yu¹²,

S. Yuan²¹, A. Yuncu⁹⁴, V. Zaccaro²⁴, C. Zampolli³³, F. Zanone⁹⁴, N. Zardoshti³³,
 A. Zarochentsev¹⁴², P. Závada⁶², N. Zaviyalov¹⁴², M. Zhalov¹⁴², B. Zhang⁶, C. Zhang¹²⁹,
 L. Zhang⁴⁰, S. Zhang⁴⁰, X. Zhang⁶, Y. Zhang¹¹⁹, Z. Zhang⁶, M. Zhao¹⁰, V. Zherebchevskii¹⁴²,
 Y. Zhi¹⁰, D. Zhou⁶, Y. Zhou⁸³, J. Zhu^{97,6}, Y. Zhu⁶, S.C. Zugravel⁵⁶, N. Zurlo^{133,55}

Affiliation Notes

^I Also at: Max-Planck-Institut für Physik, Munich, Germany

^{II} Also at: Italian National Agency for New Technologies, Energy and Sustainable Economic Development (ENEA), Bologna, Italy

^{III} Also at: Dipartimento DET del Politecnico di Torino, Turin, Italy

^{IV} Also at: Department of Applied Physics, Aligarh Muslim University, Aligarh, India

^V Also at: Institute of Theoretical Physics, University of Wrocław, Poland

^{VI} Also at: An institution covered by a cooperation agreement with CERN

Collaboration Institutes

¹ A.I. Alikhanyan National Science Laboratory (Yerevan Physics Institute) Foundation, Yerevan, Armenia

² AGH University of Krakow, Cracow, Poland

³ Bogolyubov Institute for Theoretical Physics, National Academy of Sciences of Ukraine, Kiev, Ukraine

⁴ Bose Institute, Department of Physics and Centre for Astroparticle Physics and Space Science (CAPSS), Kolkata, India

⁵ California Polytechnic State University, San Luis Obispo, California, United States

⁶ Central China Normal University, Wuhan, China

⁷ Centro de Aplicaciones Tecnológicas y Desarrollo Nuclear (CEADEN), Havana, Cuba

⁸ Centro de Investigación y de Estudios Avanzados (CINVESTAV), Mexico City and Mérida, Mexico

⁹ Chicago State University, Chicago, Illinois, United States

¹⁰ China Institute of Atomic Energy, Beijing, China

¹¹ China University of Geosciences, Wuhan, China

¹² Chungbuk National University, Cheongju, Republic of Korea

¹³ Comenius University Bratislava, Faculty of Mathematics, Physics and Informatics, Bratislava, Slovak Republic

¹⁴ COMSATS University Islamabad, Islamabad, Pakistan

¹⁵ Creighton University, Omaha, Nebraska, United States

¹⁶ Department of Physics, Aligarh Muslim University, Aligarh, India

¹⁷ Department of Physics, Pusan National University, Pusan, Republic of Korea

¹⁸ Department of Physics, Sejong University, Seoul, Republic of Korea

¹⁹ Department of Physics, University of California, Berkeley, California, United States

²⁰ Department of Physics, University of Oslo, Oslo, Norway

²¹ Department of Physics and Technology, University of Bergen, Bergen, Norway

²² Dipartimento di Fisica, Università di Pavia, Pavia, Italy

²³ Dipartimento di Fisica dell'Università and Sezione INFN, Cagliari, Italy

²⁴ Dipartimento di Fisica dell'Università and Sezione INFN, Trieste, Italy

²⁵ Dipartimento di Fisica dell'Università and Sezione INFN, Turin, Italy

²⁶ Dipartimento di Fisica e Astronomia dell'Università and Sezione INFN, Bologna, Italy

²⁷ Dipartimento di Fisica e Astronomia dell'Università and Sezione INFN, Catania, Italy

²⁸ Dipartimento di Fisica e Astronomia dell'Università and Sezione INFN, Padova, Italy

²⁹ Dipartimento di Fisica 'E.R. Caianiello' dell'Università and Gruppo Collegato INFN, Salerno, Italy

³⁰ Dipartimento DISAT del Politecnico and Sezione INFN, Turin, Italy

³¹ Dipartimento di Scienze MIFT, Università di Messina, Messina, Italy

³² Dipartimento Interateneo di Fisica 'M. Merlin' and Sezione INFN, Bari, Italy

³³ European Organization for Nuclear Research (CERN), Geneva, Switzerland

³⁴ Faculty of Electrical Engineering, Mechanical Engineering and Naval Architecture, University of Split, Split, Croatia

³⁵ Faculty of Engineering and Science, Western Norway University of Applied Sciences, Bergen, Norway

³⁶ Faculty of Nuclear Sciences and Physical Engineering, Czech Technical University in Prague, Prague, Czech Republic

- ³⁷ Faculty of Physics, Sofia University, Sofia, Bulgaria
³⁸ Faculty of Science, P.J. Šafárik University, Košice, Slovak Republic
³⁹ Frankfurt Institute for Advanced Studies, Johann Wolfgang Goethe-Universität Frankfurt, Frankfurt, Germany
⁴⁰ Fudan University, Shanghai, China
⁴¹ Gangneung-Wonju National University, Gangneung, Republic of Korea
⁴² Gauhati University, Department of Physics, Guwahati, India
⁴³ Helmholtz-Institut für Strahlen- und Kernphysik, Rheinische Friedrich-Wilhelms-Universität Bonn, Bonn, Germany
⁴⁴ Helsinki Institute of Physics (HIP), Helsinki, Finland
⁴⁵ High Energy Physics Group, Universidad Autónoma de Puebla, Puebla, Mexico
⁴⁶ Horia Hulubei National Institute of Physics and Nuclear Engineering, Bucharest, Romania
⁴⁷ Indian Institute of Technology Bombay (IIT), Mumbai, India
⁴⁸ Indian Institute of Technology Indore, Indore, India
⁴⁹ INFN, Laboratori Nazionali di Frascati, Frascati, Italy
⁵⁰ INFN, Sezione di Bari, Bari, Italy
⁵¹ INFN, Sezione di Bologna, Bologna, Italy
⁵² INFN, Sezione di Cagliari, Cagliari, Italy
⁵³ INFN, Sezione di Catania, Catania, Italy
⁵⁴ INFN, Sezione di Padova, Padova, Italy
⁵⁵ INFN, Sezione di Pavia, Pavia, Italy
⁵⁶ INFN, Sezione di Torino, Turin, Italy
⁵⁷ INFN, Sezione di Trieste, Trieste, Italy
⁵⁸ Inha University, Incheon, Republic of Korea
⁵⁹ Institute for Gravitational and Subatomic Physics (GRASP), Utrecht University/Nikhef, Utrecht, Netherlands
⁶⁰ Institute of Experimental Physics, Slovak Academy of Sciences, Košice, Slovak Republic
⁶¹ Institute of Physics, Homi Bhabha National Institute, Bhubaneswar, India
⁶² Institute of Physics of the Czech Academy of Sciences, Prague, Czech Republic
⁶³ Institute of Space Science (ISS), Bucharest, Romania
⁶⁴ Institut für Kernphysik, Johann Wolfgang Goethe-Universität Frankfurt, Frankfurt, Germany
⁶⁵ Instituto de Ciencias Nucleares, Universidad Nacional Autónoma de México, Mexico City, Mexico
⁶⁶ Instituto de Física, Universidade Federal do Rio Grande do Sul (UFRGS), Porto Alegre, Brazil
⁶⁷ Instituto de Física, Universidad Nacional Autónoma de México, Mexico City, Mexico
⁶⁸ iThemba LABS, National Research Foundation, Somerset West, South Africa
⁶⁹ Jeonbuk National University, Jeonju, Republic of Korea
⁷⁰ Johann-Wolfgang-Goethe Universität Frankfurt Institut für Informatik, Fachbereich Informatik und Mathematik, Frankfurt, Germany
⁷¹ Korea Institute of Science and Technology Information, Daejeon, Republic of Korea
⁷² KTO Karatay University, Konya, Turkey
⁷³ Laboratoire de Physique Subatomique et de Cosmologie, Université Grenoble-Alpes, CNRS-IN2P3, Grenoble, France
⁷⁴ Lawrence Berkeley National Laboratory, Berkeley, California, United States
⁷⁵ Lund University Department of Physics, Division of Particle Physics, Lund, Sweden
⁷⁶ Nagasaki Institute of Applied Science, Nagasaki, Japan
⁷⁷ Nara Women's University (NWU), Nara, Japan
⁷⁸ National and Kapodistrian University of Athens, School of Science, Department of Physics, Athens, Greece
⁷⁹ National Centre for Nuclear Research, Warsaw, Poland
⁸⁰ National Institute of Science Education and Research, Homi Bhabha National Institute, Jatni, India
⁸¹ National Nuclear Research Center, Baku, Azerbaijan
⁸² National Research and Innovation Agency - BRIN, Jakarta, Indonesia
⁸³ Niels Bohr Institute, University of Copenhagen, Copenhagen, Denmark
⁸⁴ Nikhef, National institute for subatomic physics, Amsterdam, Netherlands
⁸⁵ Nuclear Physics Group, STFC Daresbury Laboratory, Daresbury, United Kingdom
⁸⁶ Nuclear Physics Institute of the Czech Academy of Sciences, Husinec-Řež, Czech Republic
⁸⁷ Oak Ridge National Laboratory, Oak Ridge, Tennessee, United States
⁸⁸ Ohio State University, Columbus, Ohio, United States
⁸⁹ Physics department, Faculty of science, University of Zagreb, Zagreb, Croatia

- ⁹⁰ Physics Department, Panjab University, Chandigarh, India
⁹¹ Physics Department, University of Jammu, Jammu, India
⁹² Physics Program and International Institute for Sustainability with Knotted Chiral Meta Matter (SKCM2), Hiroshima University, Hiroshima, Japan
⁹³ Physikalisches Institut, Eberhard-Karls-Universität Tübingen, Tübingen, Germany
⁹⁴ Physikalisches Institut, Ruprecht-Karls-Universität Heidelberg, Heidelberg, Germany
⁹⁵ Physik Department, Technische Universität München, Munich, Germany
⁹⁶ Politecnico di Bari and Sezione INFN, Bari, Italy
⁹⁷ Research Division and ExtreMe Matter Institute EMMI, GSI Helmholtzzentrum für Schwerionenforschung GmbH, Darmstadt, Germany
⁹⁸ Saga University, Saga, Japan
⁹⁹ Saha Institute of Nuclear Physics, Homi Bhabha National Institute, Kolkata, India
¹⁰⁰ School of Physics and Astronomy, University of Birmingham, Birmingham, United Kingdom
¹⁰¹ Sección Física, Departamento de Ciencias, Pontificia Universidad Católica del Perú, Lima, Peru
¹⁰² Stefan Meyer Institut für Subatomare Physik (SMI), Vienna, Austria
¹⁰³ SUBATECH, IMT Atlantique, Nantes Université, CNRS-IN2P3, Nantes, France
¹⁰⁴ Sungkyunkwan University, Suwon City, Republic of Korea
¹⁰⁵ Suranaree University of Technology, Nakhon Ratchasima, Thailand
¹⁰⁶ Technical University of Košice, Košice, Slovak Republic
¹⁰⁷ The Henryk Niewodniczanski Institute of Nuclear Physics, Polish Academy of Sciences, Cracow, Poland
¹⁰⁸ The University of Texas at Austin, Austin, Texas, United States
¹⁰⁹ Universidad Autónoma de Sinaloa, Culiacán, Mexico
¹¹⁰ Universidade de São Paulo (USP), São Paulo, Brazil
¹¹¹ Universidade Estadual de Campinas (UNICAMP), Campinas, Brazil
¹¹² Universidade Federal do ABC, Santo Andre, Brazil
¹¹³ University of Cape Town, Cape Town, South Africa
¹¹⁴ University of Derby, Derby, United Kingdom
¹¹⁵ University of Houston, Houston, Texas, United States
¹¹⁶ University of Jyväskylä, Jyväskylä, Finland
¹¹⁷ University of Kansas, Lawrence, Kansas, United States
¹¹⁸ University of Liverpool, Liverpool, United Kingdom
¹¹⁹ University of Science and Technology of China, Hefei, China
¹²⁰ University of South-Eastern Norway, Kongsberg, Norway
¹²¹ University of Tennessee, Knoxville, Tennessee, United States
¹²² University of the Witwatersrand, Johannesburg, South Africa
¹²³ University of Tokyo, Tokyo, Japan
¹²⁴ University of Tsukuba, Tsukuba, Japan
¹²⁵ University Politehnica of Bucharest, Bucharest, Romania
¹²⁶ Université Clermont Auvergne, CNRS/IN2P3, LPC, Clermont-Ferrand, France
¹²⁷ Université de Lyon, CNRS/IN2P3, Institut de Physique des 2 Infinis de Lyon, Lyon, France
¹²⁸ Université de Strasbourg, CNRS, IPHC UMR 7178, F-67000 Strasbourg, France, Strasbourg, France
¹²⁹ Université Paris-Saclay, Centre d'Etudes de Saclay (CEA), IRFU, Département de Physique Nucléaire (DPhN), Saclay, France
¹³⁰ Université Paris-Saclay, CNRS/IN2P3, IJCLab, Orsay, France
¹³¹ Università degli Studi di Foggia, Foggia, Italy
¹³² Università del Piemonte Orientale, Vercelli, Italy
¹³³ Università di Brescia, Brescia, Italy
¹³⁴ Variable Energy Cyclotron Centre, Homi Bhabha National Institute, Kolkata, India
¹³⁵ Warsaw University of Technology, Warsaw, Poland
¹³⁶ Wayne State University, Detroit, Michigan, United States
¹³⁷ Westfälische Wilhelms-Universität Münster, Institut für Kernphysik, Münster, Germany
¹³⁸ Wigner Research Centre for Physics, Budapest, Hungary
¹³⁹ Yale University, New Haven, Connecticut, United States
¹⁴⁰ Yonsei University, Seoul, Republic of Korea
¹⁴¹ Zentrum für Technologie und Transfer (ZTT), Worms, Germany
¹⁴² Affiliated with an institute covered by a cooperation agreement with CERN

¹⁴³ Affiliated with an international laboratory covered by a cooperation agreement with CERN.